

Planning ride-sharing services with detour restrictions for spatially heterogeneous demand: A multi-zone queuing network approach

Yining Liu, Yanfeng Ouyang*

Department of Civil and Environmental Engineering, University of Illinois at Urbana-Champaign, Urbana, IL 61801, USA

Abstract

This study presents a multi-zone queuing network model for steady-state ride-sharing operations that serve heterogeneous demand, and then builds upon this model to optimize the design of ride-sharing services. Spatial heterogeneity is addressed by partitioning the study region into a set of relatively homogeneous zones, and a set of criteria are imposed to avoid significant detours among matched passengers. A generalized multi-zone queuing network model is then developed to describe how vehicles' states transition within each zone and across neighboring zones, and how passengers are served by idle or partially occupied vehicles. A large system of equations is constructed based on the queuing network model to analytically evaluate steady-state system performance. Then, we formulate a constrained nonlinear program to optimize the design of ride-sharing services, such as zone-level vehicle deployment, vehicle routing paths, and vehicle rebalancing operations. A customized solution approach is also proposed to decompose and solve the optimization problem. The proposed model and solution approach are applied to a hypothetical case and a real-world Chicago case study, so as to demonstrate their applicability and to draw insights. These numerical examples not only reveal interesting insights on how ride-sharing services serve heterogeneous demand, but also highlight the importance of addressing demand heterogeneity when designing ride-sharing services.

Keywords: Demand-responsive services, ride-sharing, detour, spatial heterogeneity, queuing network, rebalancing

1. Introduction

The advancement of wireless communication technologies has fueled the booming growth of demand-responsive services offered by transportation network companies (TNCs), e.g., Uber, Lyft, Didi, and Ola. Ride-sharing is one of the most popular services in the market, as it matches drivers and passengers with similar spatiotemporal characteristics at short notice. Individual participants may detour from their shortest paths, but they can potentially reduce their own costs by sharing the expenses with matched participants. At the societal level, properly operated ride-sharing services are expected to increase vehicle occupancy, alleviate congestion, and reduce emissions (Caulfield,

*Corresponding author. Tel: +1 217 333 9858

Email address: yfouyang@illinois.edu (Yanfeng Ouyang)

2009; Chan and Shaheen, 2012; Furuhata et al., 2013; Li et al., 2016; Yu et al., 2017; Alisoltani et al., 2021).

In the literature, the term ride-sharing has been used broadly to represent a spectrum of similar services; e.g., the driver may have a travel need (Wang et al., 2018; Wang and Yang, 2019) or provide dedicated chauffeur service, and the passenger may share the ride with the driver only (Chen et al., 2019; Özkan and Ward, 2020) or with one or more other passengers (Daganzo and Ouyang, 2019a; Bei and Zhang, 2018). In this paper, we focus on chauffeured services that can be shared by more than one passenger (also referred to as ride-splitting or shared taxi), e.g., UberPool, Lyft Line, and Didi ExpressPool.

Ride-sharing services face many similar challenges as the non-shared services (such as conventional taxi and crowd-sourcing services); e.g., the travel demand in cities usually exhibits high levels of spatial heterogeneity, and the imbalance of trip origins and destinations requires a large number of service vehicles to be systematically reallocated regularly. Most studies in the existing literature exclusively focus on non-shared services. For example, pricing strategies have been thoroughly studied as an instrument to manage demand and supply: on the demand side, the platform uses OD-based prices to induce or suppress trip demand in certain areas; on the supply side, drivers are incentivized to relocate to desired areas. Different mechanisms are developed to incentivize vehicles for relocation, e.g., adjusting the trip fare to distinguish the driver’s expected earning in different zones (Li et al., 2021), or providing an additional compensation or subsidy (Bimpikis et al., 2019; Zhu et al., 2021; Chen et al., 2021; Afifah and Guo, 2022). More recently, Xu et al. (2021a) models network equilibrium and investigates the impacts of idle trips and deadheading trips of the ride-sourcing service on network traffic congestion. Xu et al. (2021b) develops a fluid model to capture the system dynamics of ride-sourcing services, and uses it as the basis to optimize TNC pricing, matching, and vehicle dispatching decisions.

However, ride-sharing services also face new challenges, which come exactly from the sharing of rides – a new passenger may be picked up by a vehicle already serving another passenger. These passengers have different origins, destinations, or desired departure times. Pooling them into a shared vehicle most likely will create extra waiting and/or detours, and these inconveniences in turn directly affect these passengers’ willingness to use such a service (Krueger et al., 2016; Chen et al., 2017; Storch et al., 2021). Hence, it is critical to design effective passenger matching algorithms or strategies to avoid significant waiting or detours. In so doing, a large body of studies have focused on optimizing ride-sharing services, mainly at the operational level, e.g., dynamic matching algorithms (Santi et al., 2014; Alonso-Mora et al., 2017; Di Febbraro et al., 2013; Bei and Zhang, 2018; Zeng et al., 2020), and demand management and pricing (Ke et al., 2020; Jacob and Roet-Green, 2021; Zhu et al., 2020). Readers are referred to Tafreshian et al. (2020) for a comprehensive review of recent efforts.

In contrast, there are relatively few models that address the planning of ride-sharing systems. Recently, Daganzo and Ouyang (2019a) proposed an overarching modeling framework that can cover a range of demand-responsive services (e.g., taxi, ride-sharing, and dial-a-ride), and analytically connect (in closed-form formulas) TNCs’ fleet deployment decisions to passengers’ expected steady-state travel experience. Later, this modeling framework is generalize in a series of studies to address ridesharing-related challenges, e.g., restricting the detour and waiting time of matched passengers (Daganzo et al., 2020; Ouyang et al., 2021), and integrating the ride-sharing service into transit network design (Liu and Ouyang, 2021).

These above-mentioned studies on strategic planning of ride-sharing services have generally

assumed spatially homogeneous demand, probably because it is far more complex to predict how passengers from heterogeneous neighborhoods share rides: now, partially-occupied vehicles passing a certain neighborhood can join the local idle vehicles in serving arriving passengers, and hence how these vehicles are routed across neighborhoods, and how they are probabilistically matched with passengers under waiting/detour limits, would make a significant difference. The closest literature we can find address operational level decisions in this regard. For example, path-based pricing schemes are proposed, based on dynamic programming, to optimize TNCs' pricing and vehicle path decisions for ride-sharing (Lei et al., 2020) and dial-a-ride services (Shen et al., 2021). Yet, to the authors' best knowledge, the problem of strategically planning ride-sharing services to serve spatially heterogeneous demand has not been covered in the existing literature.

In light of the challenges mentioned above, this paper aims to build a steady-state ride-sharing service model for spatially heterogeneous demand, and use it to optimize the design of the ride-sharing service. The TNC needs to determine the spatial deployment of vehicles, their zone-level routes during service, the matching among vehicles and passengers, and the strategic rebalancing of idle vehicles. We first address spatial heterogeneity by partitioning the region into a set of zones, and propose a set of detour/waiting criteria for the ride-sharing service to match different types of passenger trips within and across zones. Then, we extend the aspatial queuing network model in Daganzo and Ouyang (2019a) and Daganzo et al. (2020) into a multi-zone version to describe the steady-state ride-sharing operations, which contains a set of vehicle states (characterized by a vehicle's workload and location) and a set of vehicle state transitions inside a zone (driven by passenger pickup, drop-off, and assignment events) and across zones (driven by vehicle crossing zone boundaries). A large system of nonlinear equations is formulated to connect the vehicle count in each state and the state transition flow rates, based on vehicle flow conservation within and across zones, vehicle-passenger matching criteria, and the expected duration of each vehicle state. The solution to the system of equations can be used to estimate expected system performance (such as a passenger's expected travel time). Hence, these equations are further embedded into a constrained nonlinear program so that TNCs can make optimal vehicle deployment, routing, and rebalancing decisions to minimize the average system-wide cost. A customized solution approach is also proposed to decompose and effectively solve the optimization problem.

The proposed model and solution approach are implemented in a series of hypothetical cases with varying levels of demand heterogeneity, to demonstrate their applicability and to cast insights into the optimal system characteristics. Idle vehicles and partially-occupied vehicles are found to complement each other in providing services, and for this exact reason, the relative locations of high- or low-demand zones tend to influence the volume of passing vehicles as well as idle vehicle deployments. In general, when demand is highly heterogeneous, TNCs can deploy fewer vehicles because it is easier to match riders under more concentrated demand, but more of these vehicles must be in rebalancing activities. Further comparison with a benchmark service design (optimized while ignoring demand heterogeneity) shows that the optimal service design from the proposed model can reduce the system-wide cost by about 25% \sim 30% for the selected example scenarios. This highlights the importance of properly addressing demand heterogeneity when designing ride-sharing services. In addition, we also apply the proposed model to design ride-sharing services in downtown and suburban Chicago, where trip rates vary by orders of magnitude, to demonstrate its applicability to real-world applications.

The remainder of this paper is organized as follows. Section 2 describes the multi-zone version of the queuing network model, including the matching criteria, the system of equations, the

performance metrics, the constrained non-linear program formulation, and the suggested solution approach. Section 3 presents two numerical experiments, including a hypothetical case and a Chicago case study, and discusses managerial insights. Section 4 concludes the paper and discusses possible future extensions.

2. Methodology

2.1. Model Setting

We assume that a transportation network company (TNC) needs to provide ride-sharing services to inelastic and spatially heterogeneous demand in a study region. A dense grid of streets covers the region, and service vehicles can travel on the street network along the E-W or N-S direction. Here, we let E, NE, N, NW, W, SW, S, and SE stand for East, Northeast, North, Northwest, West, Southwest, South, and Southeast directions, respectively. The region is simply connected¹ and can be approximated by a set of relatively homogeneous square zones, each with side length Φ [km]. Figure 1a shows an example, in which the study region is approximated by a grid of 16 zones. Let \mathcal{K} denote the set of zones, i.e., $\mathcal{K} = \{1, 2, \dots, |\mathcal{K}|\}$. The shortest distance between the centroids of zones i and j via the street network is denoted by L_{ij} [km]; e.g., $L_{5,13} = L_{13,5} = 3\Phi$ in Figure 1a. We define A_i^r to be the index of the adjacent zone on the r side of zone i , where $r \in \{E, N, W, S\}$, and $A_i^r = 0$ (i.e., index for a dummy zone, added for modeling convenience) if no such a zone exists. In Figure 1a, for zone 6, $A_6^E = 0$, $A_6^N = 9$, $A_6^W = 5$, and $A_6^S = 3$. Furthermore, zones are grouped based on their relative positions to each zone $i \in \mathcal{K}$. We let G_i^r denote the indices of zones in the r direction of zone i , where $r \in \{E, NE, N, NW, W, SW, S, SE\}$. Figure 1b shows an illustration, where for example $G_8^E = \{9, 10\}$ and $G_8^{NE} = \{13, 14, 16\}$. A table of key notation is summarized in Appendix A.

The generation rate of trips going from zone $i \in \mathcal{K}$ to zone $j \in \mathcal{K}$ is represented by λ_{ij} [trip/hr]. Within each zone, the origins and destinations (OD) of all its associated trips are generated from a homogeneous Poisson process over space and time. All travelers have the same value of time β [\$/veh-hr]. The TNC uses a fleet of service vehicles driven by fully compliant drivers (e.g., salaried drivers or robo-taxis). Each vehicle travels at a constant speed v [km/h], and the time for passenger boarding and alighting from a vehicle is negligible. The total hourly vehicle cost (including driver salary, prorated vehicle acquisition and operation costs) is denoted as γ [\$/veh-hr].

The TNC needs to make a range of planning decisions. First, it must determine the allocation of idle vehicles across zones. Second, it must plan the zone-level paths for vehicles traveling between every OD zone pair — since the travel demand is heterogeneous across zones, a vehicle’s path may affect its probability to encounter a passenger en-route. Here, we assume that the TNC platform only considers vehicle paths that do not have zone-level detours (Lei et al., 2020); i.e., no vehicle service path can simultaneously contain zone-level movements in both north and south (or east and west) directions. For example, in Figure 1a, the blue vehicle paths are feasible, but the red ones are not allowed. Third, it must have a plan to rebalance idle vehicles between zones because the incoming and outgoing trip generation rates of a zone could differ.

¹If the study region is not simply connected (i.e., containing “holes”), the general modeling framework is still applicable, but the definition of vehicle travel directions and the estimate of travel distance should be carefully revised. This topic will be left for future research.

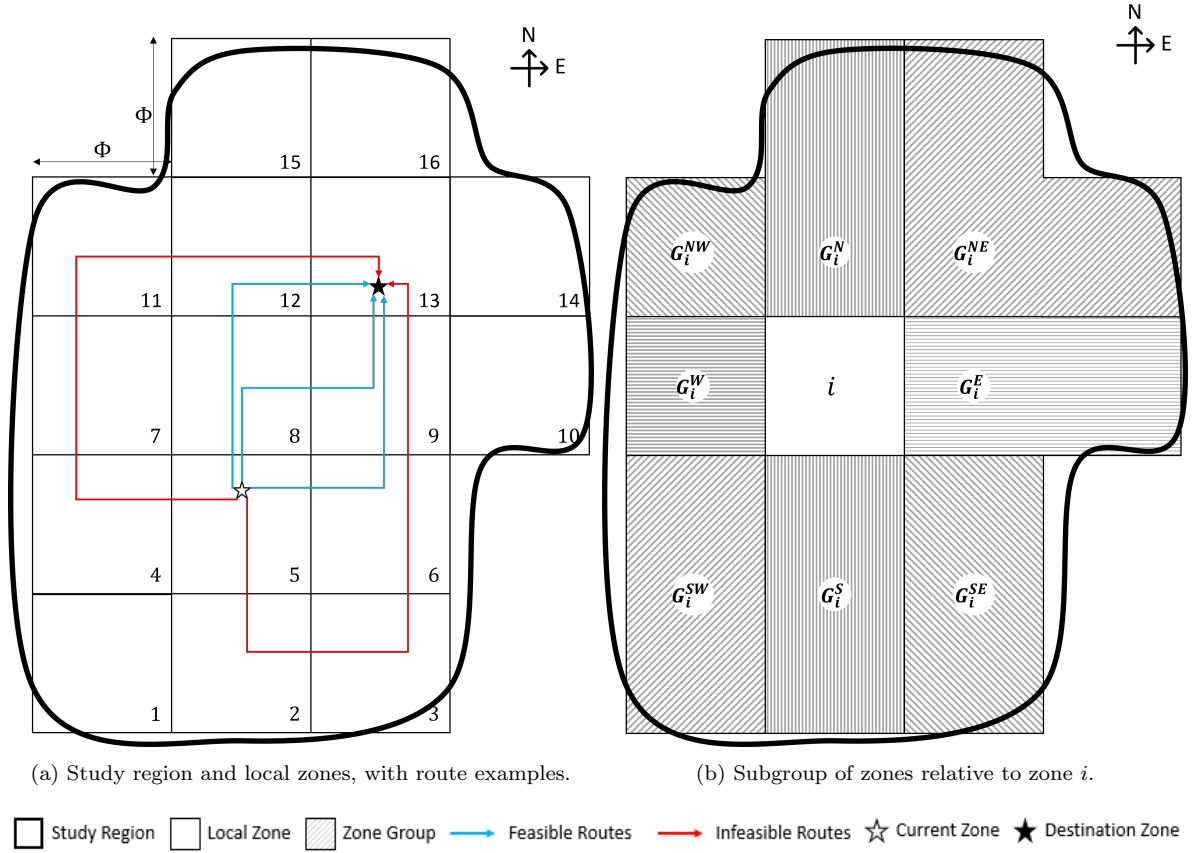
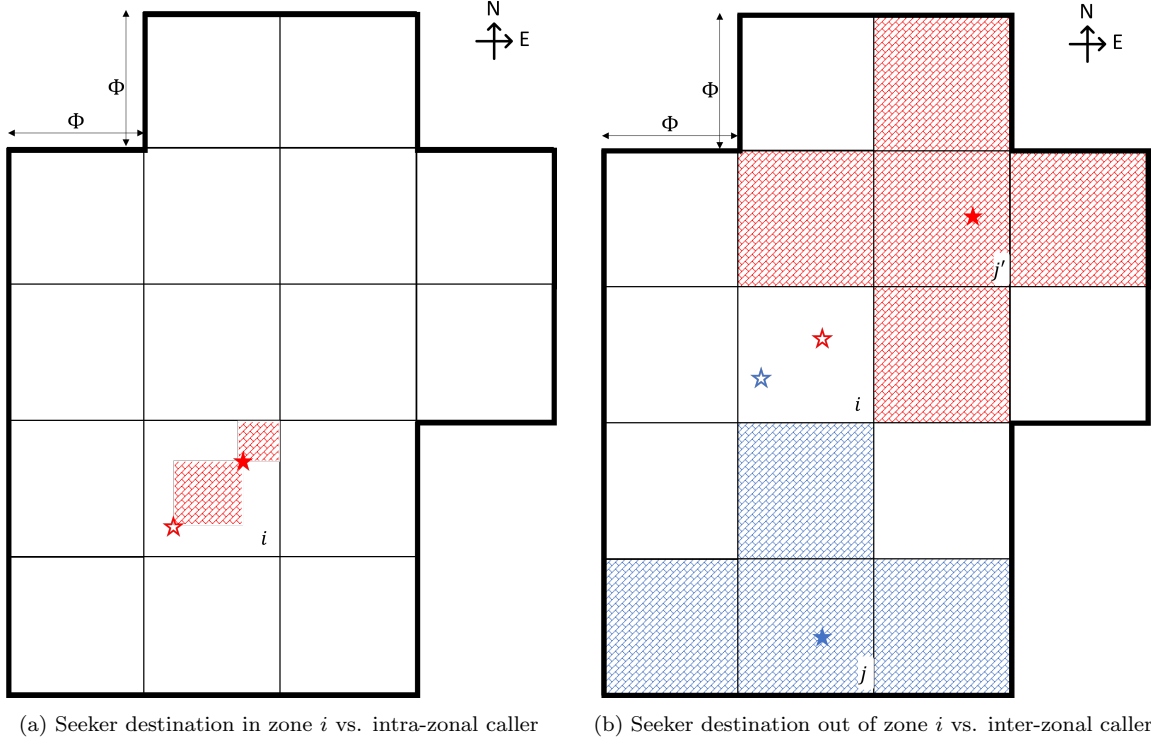


Figure 1: Illustration of study region, local zones, and zone groups.

In this study, we assume that the TNC platform adopts the following operating strategies.² When a new passenger shows up in a zone $i \in \mathcal{K}$, the TNC platform will instantly assign this passenger to a nearest “suitable” vehicle within the same zone i . No vehicle will be used to serve more than two passengers at any time (either for pickup or drop-off); in addition, no new passenger will be assigned to a vehicle already en-route to pick up another passenger (otherwise, the passengers may experience an excessive wait). As a result, the vehicles suitable for a new passenger in zone i include idle vehicles and those with one passenger on-board inside zone i . As in Daganzo and Ouyang (2019b) and Daganzo et al. (2020), the new passenger is referred to as a “caller” (i.e., one who calls for service), and the single onboard passenger of a vehicle is referred to as a “seeker” (i.e., one who seeks another rider), respectively. If the caller is assigned to an idle vehicle, the idle vehicle immediately moves toward the caller’s origin, and the caller becomes a seeker upon pickup. Otherwise, we say that the caller and the seeker are “matched,” and the vehicle with the seeker will detour from its original path to pick up the assigned caller before dropping off the seeker; upon pickup, the vehicle has two passengers onboard, and will next deliver the passenger with a closer destination (which could be within the current zone i or in another zone $j \in \mathcal{K} \setminus \{i\}$). Note that

²These assumptions aim at reducing passengers’ out-of-vehicle waiting time and limiting service detours. They can be nevertheless altered, as shown in Daganzo and Ouyang (2019b) and Daganzo et al. (2020), without affecting the structure and validity of the overarching modeling framework.



Study Region
 Local Zone
★★ Caller Origins
★★ Caller Destinations
 Seeker Destination Feasible Area

Figure 2: Feasible area for a seeker’s destination under detour restriction rules given a caller’s OD. (It should be noted that an intra-zonal caller’s OD is continuously distributed in a local zone, and it could travel in NE, NW, SW, and SE directions; the destination zone of an inter-zonal caller could be in the E, NE, N, NW, W, SW, S, and SE directions. In the following, as an illustration, we present the detour requirements for one representative direction of an intra-zonal caller (NE) and two representative directions of an inter-zonal caller (S and NE). The matching criteria for other directions shall be obvious from symmetry.)

with the above rules, vehicles with an assigned passenger cannot cross zone borders.

However, not all nearby vehicles with a seeker are suitable to serve a caller, since long detours will occur if the destination of the caller is far away from that of the seeker. We assume that the TNC imposes case-dependent limits on possible detours from a caller’s origin to the destinations of both this caller and a seeker.³ These rules, as summarized next, yield the seeker destination feasible area for any caller; i.e., if a seeker’s destination is within this area, it is eligible to be matched with this caller.

Case 1: When the seeker’s destination is within the current zone of the vehicle, i , and the caller’s trip is intra-zonal: we do not allow any detour because both passengers’ remaining trips are short; see the shaded area in Figure 2a for an illustration of the seeker destination feasible area. .

³No distance limit is imposed on the trip from a vehicle (either an idle vehicle or one with a seeker) to this caller, because we want to ensure that all callers receive service. This assumption can be relaxed, however, without affecting the overall modeling framework.

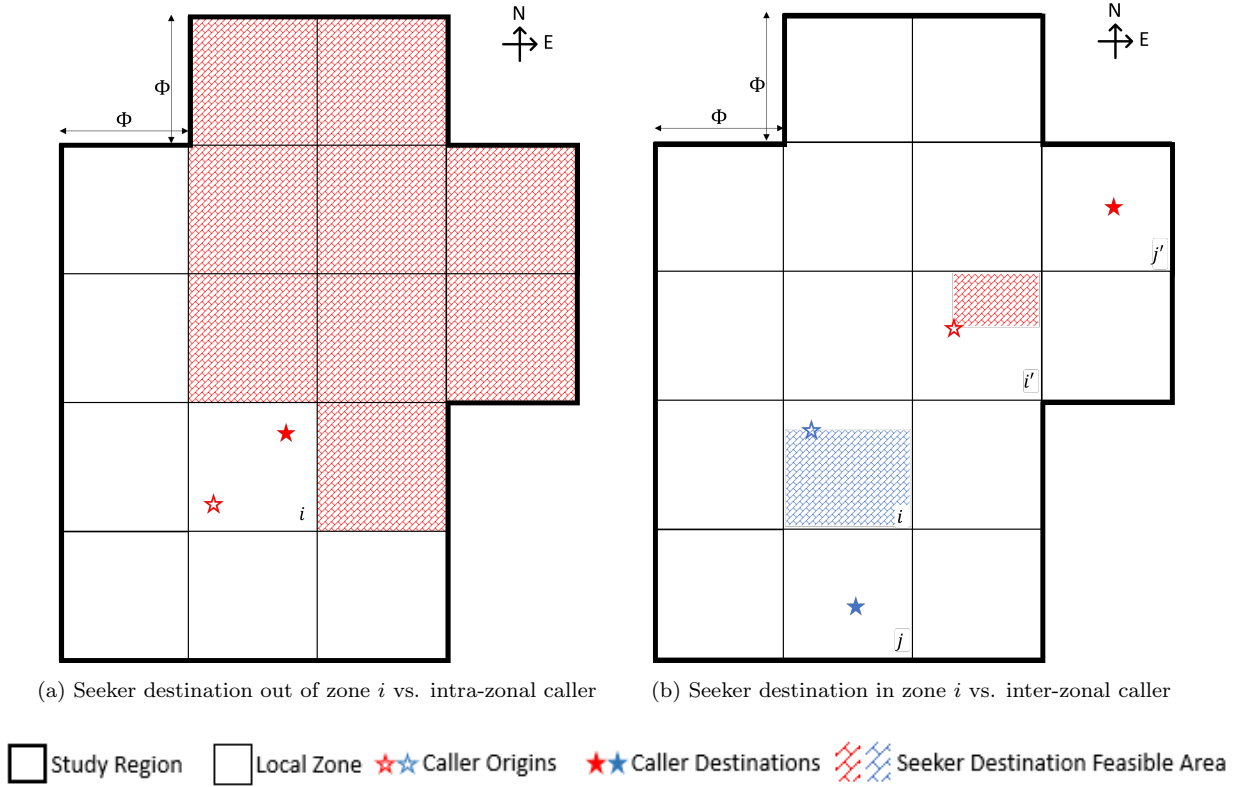


Figure 3: Feasible area for seeker's destination under detour restriction rules given a caller's OD (Part II).

- Case 2: When the seeker's destination is outside of zone i , and the caller's trip is inter-zonal toward a different zone j : we only allow detours inside local zones, but not at the zone level. For any given caller's OD zone pair (i, j) , this feasible area is fixed. Figure 2b, for example, illustrates the destination feasible areas for a seeker going in the S direction (shaded blue) and one going in the NE direction (shaded red), respectively.
- Case 3: When the seeker's destination is outside of zone i , but the caller's trip is intra-zonal: we allow local detours but require the travel directions of the seeker and the caller to be aligned. This rule avoids trapping the seeker in a local zone due to (possible) repeated pickups/deliveries of intra-zonal callers. As shown in Figure 3a, if the caller travels in the NE direction, it can only be matched with a seeker whose destination zone j is in the N, E, or NE directions of the current zone i ; i.e., $j \in G_i^N \cup G_i^{NE} \cup G_i^E$.
- Case 4: When the seeker's destination is within zone i , and the caller's trip is inter-zonal: the same rule as that for Case 3 is applied to reduce the caller's detours after it is picked up by the vehicle. Under this rule, the vehicle will travel in a direction aligned with the caller's destination while delivering the seeker. The feasible area for the seeker's destination is the part of the current zone that is to the corresponding direction of the caller's destination; see the shaded areas in Figure 3b for two examples, respectively, when the caller goes south (blue) and northeast (red).

Before building the model, we further define a few sets that can help characterize the relative

positions of the zones. First, we let $\mathcal{V}_{ij} \subseteq \{A_i^E, A_i^N, A_i^W, A_i^S\}$ as the set of zones that a vehicle in zone i heading to zone j may enter immediately after leaving zone i without zone-level detours. For example, when $j \in G_i^{\text{NE}}$, we have $\mathcal{V}_{ij} = \{A_i^N, A_i^E\}$; when $j \in G_i^N$, we have $\mathcal{V}_{ij} = \{A_i^N\}$. To simplify the expression, we define U^r as the set of two directions adjacent to direction r , i.e.,

$$\begin{aligned} U^E &= \{\text{SE}, \text{NE}\}, \quad U^{\text{NE}} = \{\text{E}, \text{N}\}, \quad U^N = \{\text{NE}, \text{NW}\}, \quad U^{\text{NW}} = \{\text{N}, \text{W}\}, \\ U^W &= \{\text{NW}, \text{SW}\}, \quad U^{\text{SW}} = \{\text{W}, \text{S}\}, \quad U^S = \{\text{SW}, \text{SE}\}, \quad U^{\text{SE}} = \{\text{S}, \text{E}\}, \end{aligned} \quad (1)$$

and therefore, we can express the feasible travel directions as follows,

$$\begin{aligned} \mathcal{V}_{ij} &= \{A_i^r\}, & \forall i \in \mathcal{K}, j \in G_i^r, r \in \{\text{E}, \text{N}, \text{W}, \text{S}\} \\ \mathcal{V}_{ij} &= \{A_i^{r'} | r' \in U^r\}. & \forall i \in \mathcal{K}, j \in G_i^r, r \in \{\text{NE}, \text{NW}, \text{SW}, \text{SE}\} \end{aligned} \quad (2)$$

Next, we define Ω_{ij} to be the set of zones in the seeker's destination feasible area when the caller is inter-zonal traveling from zone i to zone $j \in \mathcal{K} \setminus \{i\}$. For example, if a caller travels from zone 5 to zone 13 in Figure 1a, $\Omega_{5,13} = \{6, 8, 9, 12, 13, 14, 16\}$. Similarly, we define Ω_{ii}^r to be the set of zones in the destination feasible area for an intra-zonal caller traveling in the r direction, $r \in \{\text{NE}, \text{NW}, \text{SW}, \text{SE}\}$:

$$\begin{aligned} \Omega_{ii}^{\text{NE}} &= G_i^E \cup G_i^{\text{NE}} \cup G_i^N, & \Omega_{ii}^{\text{NW}} &= G_i^N \cup G_i^{\text{NW}} \cup G_i^W, \\ \Omega_{ii}^{\text{SW}} &= G_i^W \cup G_i^{\text{SW}} \cup G_i^S, & \Omega_{ii}^{\text{SE}} &= G_i^S \cup G_i^{\text{SE}} \cup G_i^E. \end{aligned} \quad (3)$$

Finally, we define $\tilde{\Omega}_{ij} = \{k \in \Omega_{ij} | L_{ik} \geq L_{ij}\}$ to be the subset of zones in the destination feasible area that are no closer to zone i than zone j . For example, $\tilde{\Omega}_{5,13} = \{13, 14, 16\}$ and $\tilde{\Omega}_{5,12} = \{11, 12, 13, 14, 15, 16\}$ in Figure 1a.

2.2. Multi-zone Queuing Network Model

We now extend the aspatial queuing network model in Daganzo and Ouyang (2019a) into a multi-zone ride-sharing version that can describe ride matching, passenger assignment, and vehicle state evolution within and across multiple zones.

2.2.1. State and Transition

The basic idea of the model is illustrated in Figure 4. We define the state of a vehicle by its current location (by zone) and its associated service task(s). Among the vehicles that are ‘‘active’’ in providing passenger service, some may be associated with no passenger at all (i.e., idling), some with one passenger (either assigned or onboard), or some with two passengers (both onboard, or one assigned and one onboard). The assigned passenger must have its origin inside the vehicle's current zone but its destination could be in any zone; similarly, each onboard passenger could have its destination in any zone. All possible states for an active vehicle in the system can be described by a vector $s = (s_0, s_1, s_2, s_3)$, where s_0 is the index of the vehicle's current zone; s_1 is the index of the origin zone of an assigned passenger, which shall take the value of s_0 if such a passenger exists (or 0 otherwise); and s_2 and s_3 respectively are the indices of the destination zones of up to two onboard passengers, if any, sorted in ascending order by the zone-level distance from the vehicle's current zone. If the vehicle has no assigned passenger, or fewer than two onboard passengers, the corresponding vector element takes the index of the dummy zone 0. Also, when the vehicle has only one onboard passenger, this passenger's destination zone is always indicated by index s_2

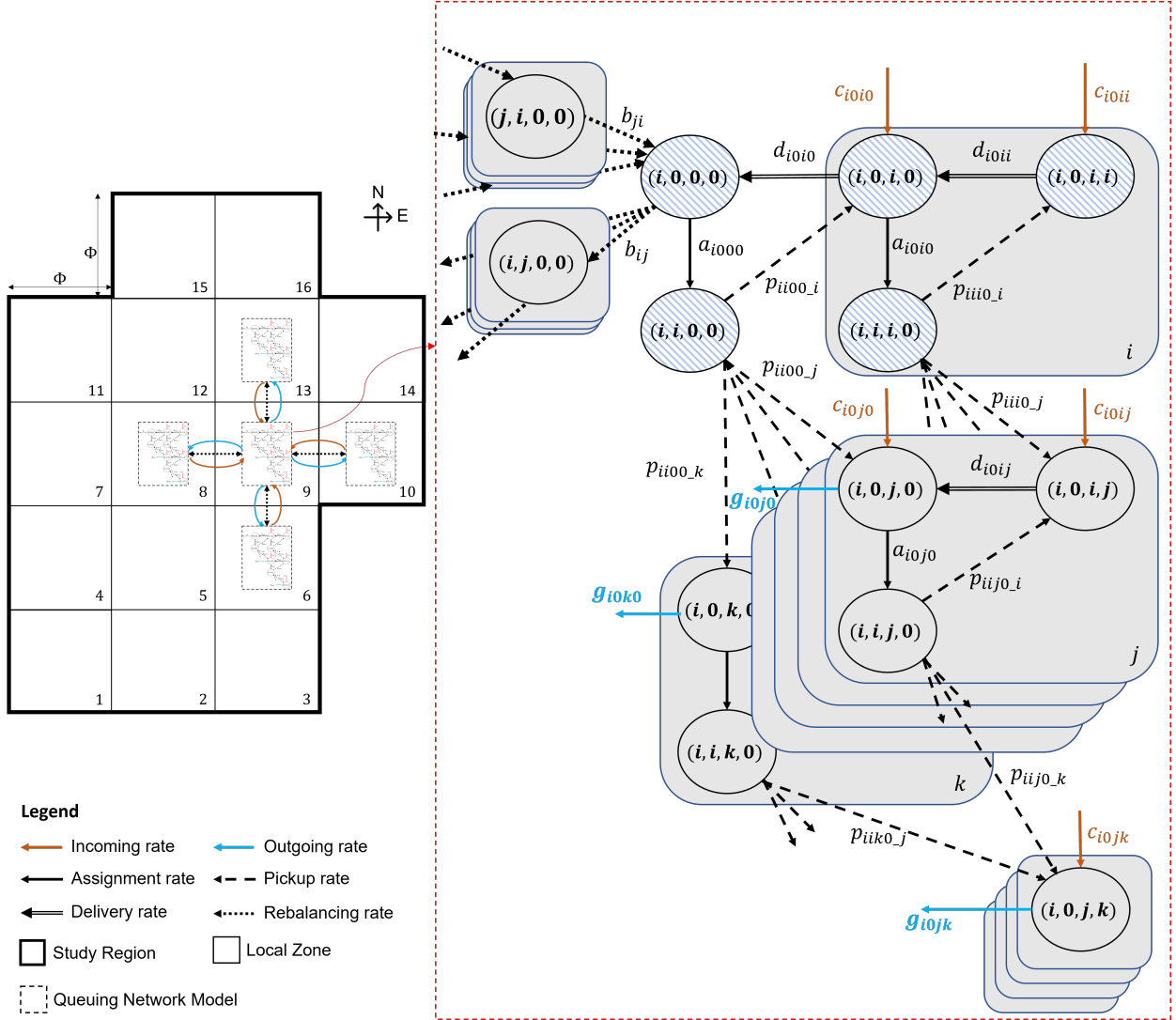


Figure 4: State transition network of a multi-zonal ride-sharing service.

(and hence $s_3 = 0$). Therefore, for active vehicles in zone $s_0 = i$, we can know that $s_1 \in \{0, i\}$, s_2 and $s_3 \in \mathcal{K} \cup \{0\}$, and s_2 and s_3 should satisfy the matching criteria from Case 1 to Case 4.

In the meantime, some vehicles cannot serve any passengers as they are being rebalanced between zones; thus, their states can be described by their origin and destination zones only, i.e., $s = (s_0, s_1, 0, 0)$, with s_0 and s_1 now being the indices of the vehicle's origin and destination zones, respectively.

The right-hand side of Figure 4 illustrates all possible vehicle states in zone i , each of which is represented by a node. Vectors $(i, j, 0, 0)$ and $(j, i, 0, 0)$ represent vehicles that are being rebalanced. All other vectors are for active vehicle states. For example, vector $(i, 0, 0, 0)$ represents the idle vehicle state; $(i, i, 0, 0)$ represents the vehicle state with one assigned caller and no onboard passenger; vectors $(i, 0, i, 0)$ and $(i, 0, j, 0)$ represent the vehicle states with one onboard seeker whose destination is in zone i and zone j , respectively; vectors $(i, i, i, 0)$ and $(i, i, j, 0)$ represent the

vehicle states with an assigned caller and a seeker destined in zone i and zone j , respectively; and vectors $(i, 0, i, i)$, $(i, 0, i, j)$, and $(i, 0, j, k)$ represent the vehicle states with two onboard passengers whose destinations are both in zone i , one in zone i and one in zone j , and one in zone j and one in zone k , respectively.

A vehicle may change its state whenever an event occurs; e.g., when it receives a new assignment, picks up an assigned caller, delivers an onboard passenger, crosses a zone boundary, or starts or ends a rebalancing trip. Each state change is represented by an arrow in the figure. Let a_s [veh/hr] denote the rate to assign callers to the vehicles in state s , illustrated by the solid arrows in Figure 4; $p_{s,i}$ [veh/hr] the rate for vehicles in state s to pick up an assigned caller with destination in zone $i \in \mathcal{K}$, illustrated by the dashed arrows; d_s [veh/hr] the rate for vehicles in state s to deliver an onboard passenger, illustrated by the double arrows; c_s (illustrated by the orange solid arrows) and g_s (illustrated by the blue solid arrows) the rates for vehicles in state s to enter and exit a zone, respectively; and b_{ij} [veh/hr] the rate for idle vehicles to be rebalanced from zone i to zone $j \in \mathcal{K} \setminus \{i\}$, as illustrated by the dotted arrows. It is noted that all aforementioned rates should be non-negative.

Figure 4 illustrates how a vehicle may change states. An idle vehicle in state $(i, 0, 0, 0)$ changes to state $(i, i, 0, 0)$ once it is assigned to a caller; such a transition occurs at rate a_{i000} . Then, the vehicle travels toward the origin of the assigned caller, who could be intra-zonal or inter-zonal.

If all callers are intra-zonal, the state- $(i, i, 0, 0)$ vehicle, upon picking up the intra-zonal caller, transitions to state $(i, 0, i, 0)$ and the caller becomes a seeker, which occurs at rate $p_{ii00.i}$. Then, this vehicle moves on to deliver the seeker toward its destination. During the delivery trip, this state- $(i, 0, i, 0)$ vehicle may receive a new assignment of a matched caller, occurring at rate a_{i0i0} , and become a state- $(i, i, i, 0)$ vehicle. In this case, the vehicle travels to pick up the assigned caller and changes to state $(i, 0, i, i)$, which occurs at rate $p_{iii0.i}$; then, as the vehicle occupancy reaches the capacity of 2, the vehicle has to deliver the passenger with a closer destination and changes to state $(i, 0, i, 0)$, occurring at rate d_{i0ii} . Otherwise, if a state- $(i, 0, i, 0)$ vehicle receives no new assignment during the delivery trip, it drops off the intra-zonal seeker at its destination, occurring at rate d_{i0i0} , after which the vehicle becomes an idle one in state $(i, 0, 0, 0)$. These types of transitions are highlighted by the top part of the network (with shaded circles) in Figure 4, which is very similar to the queuing network of single-zone ride-matching service in Daganzo et al. (2020).

The caller picked up by a vehicle in state $(i, i, 0, 0)$ or $(i, i, i, 0)$ could also be inter-zonal with its destination in zone $j \in \mathcal{K} \setminus \{i\}$. In such a case, a state- $(i, i, 0, 0)$ vehicle would change to state $(i, 0, j, 0)$ upon pickup, which occurs at rate $p_{ii00.j}$. This vehicle, while en-route toward a zone boundary to deliver the passenger, may (i) further receive a new assignment of an intra-zonal caller, and transition to states $(i, i, j, 0)$ and $(i, 0, i, j)$ and then state $(i, 0, j, 0)$ – this transition path is similar to that of vehicle state $(i, 0, i, 0)$ (as contained in a grey layer with subscript i), and may occur for all $j \in \mathcal{K} \setminus \{i\}$ (as represented by the multiple grey layers in Figure 4); (ii) receive a new assignment of an inter-zonal caller whose destination is in zone k , and transition to state $(i, 0, j, k)$; and (iii) receive no further assignment, and exit the current zone i , occurring at rate g_{i0j0} – in this case, the vehicle transitions to state $(i', 0, j, 0)$ where $i' \in \{A_i^E, A_i^N, A_i^W, A_i^S\}$ is one of zone i 's adjacent zones.

Recall that when there are two onboard passengers, we always use s_2 to denote the closer destination zone. Therefore, if an inter-zonal caller with destination in zone $j \in \mathcal{K} \setminus \{i\}$ is picked up by a vehicle in state $(i, i, i, 0)$, then the vehicle will transition to $(i, 0, i, j)$ upon pickup. Similarly,

by symmetry, a vehicle may enter state $(i, 0, j, k)$ in two ways: a state $(i, i, j, 0)$ vehicle picking up a caller with destination in zone k (at rate $p_{iij0.k}$), or a vehicle in state $(i, i, k, 0)$ picking up a caller with destination in zone j (at rate $p_{iik0.j}$). This vehicle will no longer accept new assignments but leave zone i to deliver two onboard inter-zonal passengers, at rate g_{i0jk} , and transition to state $(i', 0, j, k)$ where $i' \in \{A_i^E, A_i^N, A_i^W, A_i^S\}$.

Finally, vehicles from adjacent zones may enter or pass zone i (while delivering passengers) at certain rates; e.g., c_{i0i0} and c_{i0j0} for vehicles carrying a seeker destined in zone i and zone j , respectively; and c_{i0ii} , c_{i0ij} and c_{i0jk} for vehicles with two onboard passengers that both go to zone i , go to zone i and zone j , and go to zone j and zone k , respectively. In addition, as mentioned before, idle vehicles in the $(i, 0, 0, 0)$ state may be rebalanced to another zone $j \in \mathcal{K} \setminus \{i\}$ at rate b_{ij} , after which they transition to state $(i, j, 0, 0)$. Meanwhile, idle vehicles from zone $j \in \mathcal{K} \setminus \{i\}$ can be rebalanced to zone i at rate b_{ji} , i.e., transitioning from $(j, i, 0, 0)$ state to $(i, 0, 0, 0)$ state.

Now, in the queuing network model, we have two sets of variables, which are the transition flow rates, and the number of vehicles in each state s , denoted by $\{n_s\}$. We can build a system of equations to describe the connections among these variables in the long-term steady state. First, the vehicle state transition flow in Figure 4 should be conserved at all state nodes, such that the number of vehicles in any state $\{n_s\}$ shall remain steady. This is discussed next in Section 2.2.2. Then, we relate the flow rates and $\{n_s\}$, based on the matching criteria, assignment strategy, demand generation process, and the Little's formula; this will be discussed in Section 2.2.3.

2.2.2. Flow Conservation within and across Zones

The flow in the queuing network, as shown in Figure 4, should be conserved within each zone as well as across zones. Within a specific zone, e.g., $i \in \mathcal{K}$, the summations of the in- and out-flow at each state node must be equal. The reader can verify that the list of such conservation equations are given in Eqn. (4) below.

$$0 = \sum_{j \in \mathcal{K} \setminus \{i\}} (b_{ij} - b_{ji}) + a_{i000} - d_{i0i0}, \quad \forall i \in \mathcal{K} \quad (4.1)$$

$$0 = \sum_{j \in \mathcal{K}} p_{i00.j} - a_{i000}, \quad \forall i \in \mathcal{K} \quad (4.2)$$

$$0 = a_{i0i0} + d_{i0i0} - c_{i0i0} - d_{i0ii} - p_{i00.i}, \quad \forall i \in \mathcal{K} \quad (4.3)$$

$$0 = \sum_{j \in \mathcal{K}} p_{i00.j} - a_{i0i0}, \quad \forall i \in \mathcal{K} \quad (4.4)$$

$$0 = d_{i0ii} - p_{i00.i} - c_{i0ii}, \quad \forall i \in \mathcal{K} \quad (4.5)$$

$$0 = g_{i0j0} + a_{i0j0} - p_{i00.j} - c_{i0j0} - d_{i0ij}, \quad \forall i \in \mathcal{K}, j \in \mathcal{K} \setminus \{i\} \quad (4.6)$$

$$0 = \sum_{k \in \Omega_{ij} \cup \{i\}} p_{iij0.k} - a_{i0j0}, \quad \forall i \in \mathcal{K}, j \in \mathcal{K} \setminus \{i\} \quad (4.7)$$

$$0 = d_{i0ij} - c_{i0ij} - p_{i00.j} - p_{iij0.i}, \quad \forall i \in \mathcal{K}, j \in \mathcal{K} \setminus \{i\} \quad (4.8)$$

$$0 = g_{i0jk} - c_{i0jk} - p_{iij0.k} - \mathbb{I}(k \neq j) \cdot p_{iik0.j}, \quad \forall i \in \mathcal{K}, j \in \mathcal{K} \setminus \{i\}, k \in \tilde{\Omega}_{ij} \quad (4.9)$$

where $\mathbb{I}(k \neq j) = 1$ if $k \neq j$, or 0 otherwise; it is used to avoid counting the pickup rate $p_{iij0.j}$ twice when the destination zones of two onboard inter-zonal passengers are the same.

Vehicle flow must also be conserved across zones. Note that the outgoing flow, g , from one zone becomes incoming flow, c , of its adjacent zones. Hence, we must track how vehicles may travel across zones, and construct a relationship between the outgoing and incoming flow across zone boundaries.

Despite all feasible travel paths a vehicle could follow to reach its onboard passengers' destinations, a vehicle can only move into at most two adjacent zones without creating zone-level detours; this is specified in Eqn. (2). The platform shall choose vehicle paths, especially for those vehicles with a seeker (i.e., currently in state $(i, 0, j, 0)$), to enhance system efficiency; e.g., by impacting the probability for the vehicle to find a suitable matched caller en-route. These path decisions collectively specify the proportion of state- $(i, 0, j, 0)$ vehicles that enter a zone $i' \in \{A_i^E, A_i^N, A_i^W, A_i^S\}$ upon leaving zone i , which is denoted by $\delta_{ij-i'} \in [0, 1]$. In addition, vehicles with two onboard inter-zonal passengers (i.e., currently in state $(i, 0, j, k)$) also travel across zones to deliver passengers. The path of such a vehicle toward its closer destination zone j has no effects on the system operations (since it cannot serve other passengers en-route).⁴ Hence, we can, for simplicity, set the proportion of state- $(i, 0, j, k)$ vehicles that enter zone i' upon leaving zone i to also be $\delta_{ij-i'}$. The vehicle path decisions should satisfy the following constraints:

$$\sum_{i' \in \{A_i^E, A_i^N, A_i^W, A_i^S\}} \delta_{ij-i'} = 1, \quad \sum_{i' \in \mathcal{V}_{ij}} \delta_{ij-i'} = 1, \quad \forall i \in \mathcal{K}, j \in \mathcal{K} \setminus \{i\} \quad (5)$$

which postulate that a vehicle can only travel in a feasible direction horizontally or vertically into an adjacent zone. Then, it is easy to see that the vehicle flow across adjacent zones must satisfy the following:

$$\begin{aligned} c_{i0i0} &= \sum_{i' \in \{A_i^E, A_i^N, A_i^W, A_i^S\}} g_{i'0i0} \cdot \delta_{i'i-i}, & \forall i \in \mathcal{K} \\ c_{i0ii} &= \sum_{i' \in \{A_i^E, A_i^N, A_i^W, A_i^S\}} g_{i'0ii} \cdot \delta_{i'i-i}, & \forall i \in \mathcal{K} \\ c_{i0j0} &= \sum_{i' \in \{A_i^E, A_i^N, A_i^W, A_i^S\}} g_{i'0j0} \cdot \delta_{i'j-i}, & \forall i \in \mathcal{K}, j \in \mathcal{K} \setminus \{i\} \\ c_{i0ij} &= \sum_{i' \in \{A_i^E, A_i^N, A_i^W, A_i^S\}} g_{i'0ij} \cdot \delta_{i'i-i}, & \forall i \in \mathcal{K}, j \in \mathcal{K} \setminus \{i\} \\ c_{i0jk} &= \sum_{i' \in \{A_i^E, A_i^N, A_i^W, A_i^S\}} g_{i'0jk} \cdot \delta_{i'j-i}, & \forall i \in \mathcal{K}, j \in \mathcal{K} \setminus \{i\}, k \in \tilde{\Omega}_{ij} \end{aligned} \quad (6)$$

2.2.3. Flow Rates, Matching, and Expected Vehicle State Duration

Recall that a new caller in zone i could be assigned to a nearest suitable vehicle in states $(i, 0, 0, 0)$, $(i, 0, i, 0)$, and $(i, 0, j, 0)$, $\forall j \in \mathcal{K} \setminus \{i\}$. The caller could be inter-zonal (traveling from zone i to any zone j), or intra-zonal (traveling in any direction $r \in \{\text{NE}, \text{NW}, \text{SW}, \text{SE}\}$ within zone

⁴Note that we do not consider traffic congestion in this study; thus, the vehicle density in a local zone does not affect the travel time. If congestion is an issue, the travel directions of all types of vehicles should be carefully chosen.

i). Appendix B shows that the number of vehicles suitable to serve an intra-zonal caller traveling in direction r within zone i , denoted by N_{ii}^r , is given by

$$N_{ii}^r = n_{i000} + \frac{2n_{i0i0}}{9} + \sum_{j \in \Omega_{ii}^r} n_{i0j0}, \quad \forall i \in \mathcal{K}, r \in \{\text{NE, NW, SW, SE}\} \quad (7)$$

and the number of vehicles suitable to serve an inter-zonal caller going from zone i to zone j , denoted by N_{ij} , is given by

$$N_{ij} = n_{i000} + \frac{n_{i0i0}}{4} + \sum_{k \in \Omega_{ij}} n_{i0k0}, \quad \forall i \in \mathcal{K}, j \in G_i^r, r \in \{\text{NE, NW, SW, SE}\} \quad (8)$$

$$N_{ij} = n_{i000} + \frac{n_{i0i0}}{2} + \sum_{k \in \Omega_{ij}} n_{i0k0}, \quad \forall i \in \mathcal{K}, j \in G_i^r, r \in \{\text{E, N, W, S}\}$$

Under the nearest assignment strategy, the fraction of callers assigned to vehicles in any suitable state is proportional to the number of vehicles in that state. Appendix B further shows that $\{N_{ij}\}$ and $\{N_{ii}^r\}$ are related to the caller pickup rates as follows:

$$p_{ii00-i} = \sum_{r \in \{\text{NE, NW, SW, SE}\}} \left(\frac{\lambda_{ii}}{4} \cdot \frac{n_{i000}}{N_{ii}^r} \right), \quad \forall i \in \mathcal{K} \quad (9.1)$$

$$p_{iii0-i} = \sum_{r \in \{\text{NE, NW, SW, SE}\}} \left(\frac{\lambda_{ii}}{4} \cdot \frac{2n_{i0i0}}{9N_{ii}^r} \right), \quad \forall i \in \mathcal{K} \quad (9.2)$$

$$p_{iij0-i} = \frac{\lambda_{ii}}{4} \cdot \frac{n_{i0j0}}{N_{ii}^r}, \quad \forall i \in \mathcal{K}, j \in G_i^r, r \in \{\text{NE, NW, SW, SE}\} \quad (9.3)$$

$$p_{iij0-i} = \sum_{r \in U^{r'}} \left(\frac{\lambda_{ii}}{4} \cdot \frac{n_{i0j0}}{N_{ii}^r} \right), \quad \forall i \in \mathcal{K}, j \in G_i^{r'}, r' \in \{\text{E, N, S, W}\} \quad (9.4)$$

$$p_{ii00-j} = \lambda_{ij} \cdot \frac{n_{i000}}{N_{ij}}, \quad \forall i \in \mathcal{K}, j \in \mathcal{K} \setminus \{i\} \quad (9.5)$$

$$p_{iii0-j} = \lambda_{ij} \cdot \frac{n_{i0i0}}{4N_{ij}}, \quad \forall i \in \mathcal{K}, j \in G_i^r, r \in \{\text{NE, NW, SW, SE}\} \quad (9.6)$$

$$p_{iii0-j} = \lambda_{ij} \cdot \frac{n_{i0i0}}{2N_{ij}}, \quad \forall i \in \mathcal{K}, j \in G_i^r, r \in \{\text{E, N, S, W}\} \quad (9.7)$$

$$p_{iik0-j} = \lambda_{ij} \cdot \frac{n_{i0k0}}{N_{ij}}, \quad \forall i \in \mathcal{K}, j \in \mathcal{K} \setminus \{i\}, k \in \Omega_{ij} \quad (9.8)$$

For a vehicle in zone i with a seeker (i.e., in state $(i, 0, i, 0)$ or $(i, 0, j, 0)$), it may receive a new assignment during its delivery trip (which occurs at rate a_{i0i0} or a_{0j0i} , respectively); otherwise, the vehicle will exit the current zone with the seeker (which occurs at rate d_{i0i0} or g_{i0j0} , respectively). The probability for the latter case to occur depends on the new passenger assignment rates and the length of the delivery path inside zone i . Since new passengers arrive according to Poisson processes, Appendix C shows that the rates d_{i0i0} and g_{i0j0} , $\forall j \in \mathcal{K} \setminus \{i\}$, satisfy the following,

$$d_{i0i0} = c_{i0i0} \cdot e^{-\frac{a_{i0i0} \cdot 5\Phi}{n_{i0i0} \cdot 6v}} + (p_{i0i0_i} + c_{i0ii}) \cdot e^{-\frac{a_{i0i0} \cdot 2\Phi}{n_{i0i0} \cdot 3v}} + p_{i0i0_i} \cdot e^{-\frac{a_{i0i0} \cdot \Phi}{n_{i0i0} \cdot 2v}}, \quad (10.1)$$

$$g_{i0j0} = c_{i0j0} \cdot e^{-\frac{a_{i0j0} \cdot \Phi}{n_{i0j0} \cdot v}} + (p_{i0i0_j} + d_{i0ij}) \cdot e^{-\frac{a_{i0j0} \cdot \Phi}{n_{i0j0} \cdot 2v}}. \quad (10.2)$$

Based on Eqn. (4) and Eqn. (6)-(10), we can express the transition flow rates $\{a_s\}$, $\{p_{s_i}\}$, $\{d_{sj}\}$, $\{g_s\}$, and $\{c_s\}$ as functions of $\{n_{i000}\}$, $\{n_{i0i0}\}$, $\{n_{i0j0}\}$, δ , and $\{b_{ij}\}$. We can further use these flow rates to quantify the number of vehicles in any of the remaining states, by multiplying the expected duration of that vehicle state and the vehicle arrival rate into that state, per the Little's Law (Little, 1961). Appendix C gives detailed derivations on the expected duration in each vehicle state, which leads to the following relationships:

$$n_{ii00} = \frac{0.63\Phi n_{i000}}{v} \left(\sum_{r \in \{\text{NE, NW, SW, SE}\}} \frac{\lambda_{ii}}{4(N_{ii}^r)^{\frac{3}{2}}} + \sum_{j \in \mathcal{K} \setminus \{i\}} \frac{\lambda_{ij}}{(N_{ij})^{\frac{3}{2}}} \right), \quad \forall i \in \mathcal{K} \quad (11.1)$$

$$n_{i0i0} = \frac{0.63\Phi n_{i0i0}}{2v} \left[\sum_{r \in \{\text{NE, NW, SW, SE}\}} \left(\frac{\lambda_{ii}}{9(N_{ii}^r)^{\frac{3}{2}}} + \sum_{j \in G_i^r} \frac{\lambda_{ij}}{2(N_{ij})^{\frac{3}{2}}} \right) + \sum_{j \in G_i^E \cup G_i^N \cup G_i^W \cup G_i^S} \frac{\lambda_{ij}}{(N_{ij})^{\frac{3}{2}}} \right], \quad \forall i \in \mathcal{K} \quad (11.2)$$

$$n_{iij0} = \frac{0.63\Phi n_{i0j0}}{v} \left(\frac{\lambda_{ii}}{4(N_{ii}^r)^{\frac{3}{2}}} + \sum_{k \in \Omega_{ij}} \frac{\lambda_{ik}}{(N_{ik})^{\frac{3}{2}}} \right), \quad \forall i \in \mathcal{K}, j \in G_i^r, r \in \{\text{NE, NW, SW, SE}\} \quad (11.3)$$

$$n_{ijj0} = \frac{0.63\Phi n_{i0j0}}{v} \left(\sum_{r \in U^{r'}} \frac{\lambda_{ii}}{4(N_{ii}^r)^{\frac{3}{2}}} + \sum_{k \in \Omega_{ij}} \frac{\lambda_{ik}}{(N_{ik})^{\frac{3}{2}}} \right), \quad \forall i \in \mathcal{K}, j \in G_i^{r'}, r' \in \{E, N, W, S\} \quad (11.4)$$

$$n_{i0ii} = c_{i0ii} \cdot \frac{5\Phi}{8v} + p_{i0i0_i} \cdot \frac{\Phi}{2v}, \quad \forall i \in \mathcal{K} \quad (11.5)$$

$$n_{i0ij} = c_{i0ij} \cdot \frac{5\Phi}{6v} + (p_{i0i0_j} + p_{i0j0_i}) \cdot \frac{2\Phi}{3v}, \quad \forall i \in \mathcal{K}, j \in \mathcal{K} \setminus \{i\} \quad (11.6)$$

$$n_{i0jk} = c_{i0jk} \cdot \frac{\Phi}{v} + [p_{i0j0_k} + \mathbb{I}(k \neq j) \cdot p_{i0k0_j}] \cdot \frac{\Phi}{2v}, \quad \forall i \in \mathcal{K}, j \in \mathcal{K} \setminus \{i\}, k \in \tilde{\Omega}_{ij} \quad (11.7)$$

$$n_{ij00} = b_{ij} \cdot \frac{L_{ij}}{v}, \quad \forall i \in \mathcal{K}, j \in G_i^{\text{NE}} \cup G_i^{\text{NW}} \cup G_i^{\text{SW}} \cup G_i^{\text{SE}} \quad (11.8)$$

$$n_{ij00} = b_{ij} \cdot \frac{L_{ij} + \Phi/3}{v}, \quad \forall i \in \mathcal{K}, j \in G_i^E \cup G_i^N \cup G_i^W \cup G_i^S. \quad (11.9)$$

2.3. Performance Evaluation

With the number of vehicles in each state $\{n_s\}$, we can evaluate the system performance, including the agency cost and passenger travel experience. There are many ways to formulate the system costs; in this paper, as an illustration, we assume the agency cost is proportional to the total vehicle hours in operation, and the passenger cost is proportional to the summation of their total travel times (from calling for service to arriving at the destination).

The total number of active vehicles in zone i , denoted by M_i [veh], is

$$M_i = n_{i000} + n_{ii00} + n_{i0i0} + n_{iii0} + n_{i0ii} + \sum_{j \in \mathcal{K} \setminus \{i\}} \left(n_{i0j0} + n_{i0ij} + n_{ii j0} + \sum_{k \in \tilde{\Omega}_{ij}} n_{i0jk} \right)$$

and that of rebalanced vehicles is $M_b = \sum_{i \in \mathcal{K}} \sum_{j \in \mathcal{K} \setminus \{i\}} n_{ij00}$ [veh]. Therefore, the total fleet needed across all zones can be written as

$$M = \sum_{i \in \mathcal{K}} M_i + M_b. \quad (12)$$

This quantity is also the total vehicle hours in operation per hour, i.e., with unit veh-hr/hr. Therefore, the total agency cost per hour is simply γM \$/hr.

Also, we can calculate the total trip time spent by all passengers per hour, denoted by P [pax-hr/hr]. Its formula is based on that for M_i , except that each term n_s is weighted by the number of assigned and onboard passengers per vehicle in state s ; i.e.,

$$P = \sum_{i \in \mathcal{K}} \left[n_{ii00} + n_{i0i0} + 2(n_{iii0} + n_{i0ii}) + \sum_{j \in \mathcal{K} \setminus \{i\}} \left(n_{i0j0} + 2n_{i0ij} + 2n_{ii j0} + 2 \sum_{k \in \tilde{\Omega}_{ij}} n_{i0jk} \right) \right]. \quad (13)$$

Therefore, the total passenger cost per hour is βP \$/hr. The system-wide cost per passenger, denoted by Z [\$/pax], hence, is as follows,

$$Z = \frac{\gamma M + \beta P}{\sum_{i,j \in \mathcal{K}} \lambda_{ij}}. \quad (14)$$

2.4. Optimization Model and Solution Approach

Eqn. (4) and Eqn. (6)-(11) collectively describe how, in the steady state of the queuing network, the following variables are related: the vehicle transition flow rates $\{a_s\}$, $\{p_{s.i}\}$, $\{d_s\}$, $\{c_s\}$, $\{g_s\}$, $\{b_{ij}\}$; the vehicle counts in all states $\{n_s\}$; and vehicle path fractions $\boldsymbol{\delta}$. It can be easily verified that, conditional on any choice of $\boldsymbol{\delta}$, $\{b_{ij}\}$, and $\{n_{i000}\}$ (idle vehicle counts), all other variables can be solved from the system of equations, and so can the system performance Z . As such, the TNC can optimize their decisions of $\boldsymbol{\delta}$, $\{b_{ij}\}$, and $\{n_{i000}\}$ to minimize the system-wide cost per passenger for providing a multi-zonal ride-sharing service; i.e.,

$$\min_{\boldsymbol{\delta}, \{n_{i000}\}, \{b_{ij}\}} Z$$

$$\text{s.t. Eqn. (1) - (14)}$$

$$a_s, p_{s.i}, d_s, c_s, g_s, n_s \geq 0, \quad \forall s \quad (15)$$

$$\delta_{ij.i'} \in [0, 1], \quad \forall i \in \mathcal{K}, j \in \mathcal{K} \setminus \{i\}, i' \in \{A_i^r\}_{r \in \{E, N, W, S\}} \quad (16)$$

$$b_{ij} \geq 0, \quad \forall i \in \mathcal{K}, j \in \mathcal{K} \setminus \{i\} \quad (17)$$

where Eqn. (15) enforces all flow rates and fleet sizes to be non-negative real numbers;⁵ and Eqn. (16)-(17) specify the value domains for vehicle travel direction decisions and rebalancing flow rates.

This optimization problem involves only continuous variables, and hence it can be solved by gradient-based search methods. However, it is highly nonlinear and nonconvex, so it is challenging to directly search all involved variables simultaneously. We propose to decompose the problem by observing that the set of rebalancing flow $\{b_{ij}\}$ only appear as $\{\sum_{j \in \mathcal{K} \setminus \{i\}} (b_{ij} - b_{ji}), \forall i\}$ in the flow conservation constraint (4.1), and as a linear summation term in the objective function (see from Eqn. (11)-(12)). Given any combination of δ and $\{n_{i000}\}$, we can treat $\{\sum_{j \in \mathcal{K} \setminus \{i\}} (b_{ij} - b_{ji}), \forall i\}$ as $|\mathcal{K}|$ variables, and solve them together with $\{a_s\}$, $\{p_{s,i}\}$, $\{d_s\}$, $\{c_s\}$, $\{g_s\}$, $\{n_{i0i0}\}$, and $\{n_{i0j0}\}$, from Eqn. (4) and Eqn. (6)-(10). Then, we can solve $\{b_{ij}\}$ from a transportation problem, using $\sum_{j \in \mathcal{K} \setminus \{i\}} (b_{ij} - b_{ji})$ as the “demand” or “supply” of zone i , and L_{ij}/v or $(L_{ij} + \Phi/3)/v$ from Eqn. (11.8)-(11.9) as the shipment costs. After obtaining all flow rates, we can quantify the vehicle counts in all states based on Eqn. (11).

The basic solution algorithm can be summarized as follows.

Step 1: Randomly initialize variables δ and $\{n_{i000}\}$; set the iteration number to be 1.

Step 2: Given the current δ and $\{n_{i000}\}$, evaluate the system performance as follows.

Step 2.1: Solve Eqn. (4) and Eqn. (6)-(10) to obtain values of $\{a_s\}$, $\{p_{s,i}\}$, $\{d_s\}$, $\{c_s\}$, $\{g_s\}$, $\{n_{i0i0}\}$, $\{n_{i0j0}\}$, and $\{\sum_{j \in \mathcal{K} \setminus \{i\}} (b_{ij} - b_{ji})\}$.

Step 2.2: Use $\{\sum_{j \in \mathcal{K} \setminus \{i\}} (b_{ij} - b_{ji})\}$ as input, solve $\{b_{ij}\}$ from the transportation problem.

Step 2.3: Solve vehicle counts $\{n_s\}$ from Eqn. (11). If Eqn. (15)-(17) are satisfied, evaluate the system performance from Eqn. (12)-(14); otherwise, set $Z = \infty$.

Step 3: Record (or update) the best solution so far, if possible. Perturb δ and $\{n_{i000}\}$ by small increments, and repeat Step 2 to numerically compute the gradient. Then, conduct a gradient-based search to find a new solution δ and $\{n_{i000}\}$; increase the iteration number by 1 and go to Step 2.

Step 4: If a maximum iteration number is reached, or if the best objective value does not improve in a number of iterations, terminate the algorithm.

Before moving on to the numerical results, we suggest two optional treatments that may facilitate the solution process. First, note that the solution procedure for the system of nonlinear equations in Step 2.1 can be very sensitive to the initial guess. Therefore, we can try multiple guesses, and/or keep a memory of past solutions (i.e., from different δ and $\{n_{i000}\}$ values) as candidate initial guesses. If no solution can be found after a number of such initial guesses, then we consider this combination of δ and $\{n_{i000}\}$ to be infeasible (and set $Z = \infty$). Second, note that the cross-zone vehicle flow rates g and $\{c_{i0j0}\}$, $\{c_{i0ij}\}$, $\{c_{i0jk}\}$ are coupled through Eqn. (6) and Eqn. (10), and they are linearly related once assignment rates $\{a_s\}$ and pickup rates $\{p_{s,i}\}$ are known. Hence, it is beneficial to first calculate $\{p_{s,i}\}$ based on Eqn. (9), obtain $\{a_s\}$ with Eqn. (4), and use matrix elimination methods to solve g and $\{c_{i0j0}\}$, $\{c_{i0ij}\}$, $\{c_{i0jk}\}$ from a linear system of equation. After that, $\{c_{i,0,i,0}\}$, $\{c_{i,0,i,i}\}$, $\{d_{i,0,i,0}\}$ can also be computed.

⁵All vehicle counts in $\{n_s\}$ are interpreted as expected values, and hence we allow them to be non-negative real numbers. In large-scale systems, the presence of seekers also allows service to be still available to passengers even when idle vehicle counts in some zones approach zero.

	Zone 1			Zone 2			Zone 3			Zone 4			$\sum_i M_i$	M_b	M
	n_{1000}	$\delta_{14.2}$	$\delta_{14.3}$	n_{2000}	$\delta_{23.1}$	$\delta_{23.4}$	n_{3000}	$\delta_{32.1}$	$\delta_{32.4}$	n_{1000}	$\delta_{41.2}$	$\delta_{41.3}$			
S1	6	1.00	0.00	9	0.54	0.46	32	0.50	0.50	6	1.00	0.00	1915	486	2401
S2	4	1.00	0.00	51	0.50	0.50	51	0.50	0.50	4	1.00	0.00	1984	199	2183
S3	3	–	–	59	0.50	0.50	59	0.50	0.50	3	–	–	1999	188	2187

Table 1: Optimal service design for the hypothetical example.

3. Numerical Analysis

In this section, we first test the model with a hypothetical square region to see how the optimal service decisions and system performance vary in different demand scenarios. Later, we apply the proposed model to a real-world case study for downtown and suburban Chicago to draw further insights.

The “root” function in Scipy (Virtanen et al., 2020) is used to find the solution to the system of equations in Step 2.1. The GNU Linear Programming Kit solver (Makhorin, 2008) embedded in Pyomo (Hart et al., 2011; Bynum et al., 2021) is used to solve the transportation problem in Step 2.2. The Sequential Least Squares Programming algorithm (Kraft, 1988) implemented in Scipy (Virtanen et al., 2020) is used to conduct the gradient-based search in Step 3.

In all cases, the vehicle cruising speed is $v = 25$ km/hr, and the passengers’ value-of-time is $\beta = 20$ \$/hr. Following Liu and Ouyang (2021), the vehicle operation cost is set as $\gamma = 40 + 0.48v = 52$ \$/hr, in which 40 is the driver wages per hour, and 0.48 is the prorated vehicle cost per km for vehicle acquisition, depreciation, and fuel (Zoepf et al., 2018).

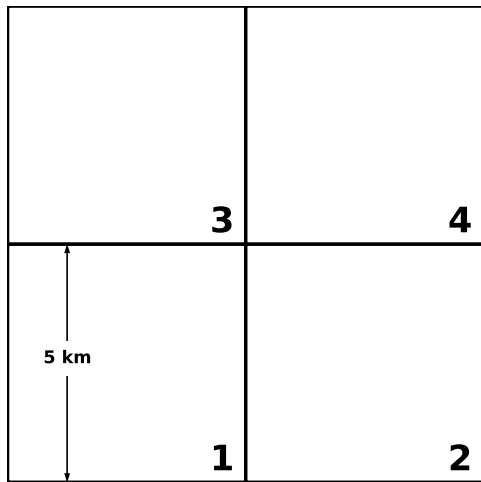
3.1. Hypothetical Case

Here, we consider a small square region that can be partitioned into 2×2 zones, each with a side length $\Phi = 5$ km, as shown in Figure 5a. We apply the proposed model to a set of heterogeneous demand scenarios, while the total trip rate is fixed at $\sum_{i,j} \lambda_{ij} = 8,000$ trip/hr: (i) scenario S1: $\lambda_{i1} = \lambda_{i2} = \lambda_{i4} = 200$ trip/hr, and $\lambda_{i3} = 1400$ trip/hr, $\forall i \in \mathcal{K}$; (ii) scenario S2: $\lambda_{i1} = \lambda_{i4} = 200$ trip/hr, $\lambda_{i2} = 600$ trip/hr, and $\lambda_{i3} = 1000$ trip/hr, $\forall i \in \mathcal{K}$; and (iii) scenario S3: $\lambda_{i1} = \lambda_{i4} = 200$ trip/hr, $\lambda_{i2} = \lambda_{i3} = 800$ trip/hr, $\forall i \in \mathcal{K}$. In each of these scenarios, the four zones have the same outgoing trip rate, but different incoming trip rates.

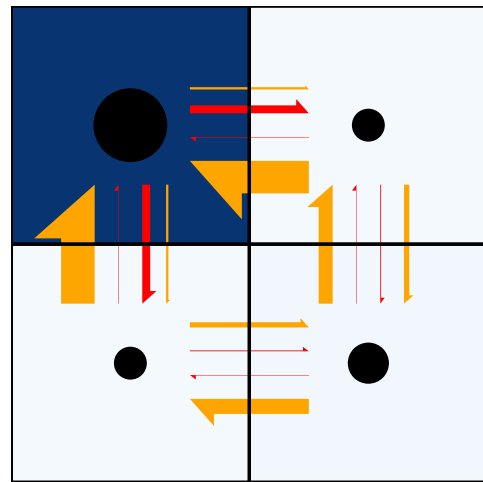
The optimal deployment of idle vehicles and vehicle travel path decisions are summarized in Table 1.⁶ Vehicle counts are rounded to be integers, and we only display the vehicle path decisions between the diagonal zone pairs (for which vehicles have two paths) — those for other zone pairs are set by Constraint (5) to take value 0 or 1. In addition, Figures 5b-5d illustrate the numbers of idle vehicles (represented by the size of the black dots) and vehicles with a seeker (represented by the background color) in each zone. It also shows the flow rates of vehicles with a seeker (represented by the thickness of red arrows) and those with two passengers (represented by the thickness of yellow arrows) between neighboring zones.

Scenario S1 mimics the morning rush in a city with a distinct CBD (i.e., zone 3). It is not surprising that this zone has the largest number of idle vehicles, because a large number of incoming vehicles become idle upon completion of passenger deliveries in this zone. Although the remaining

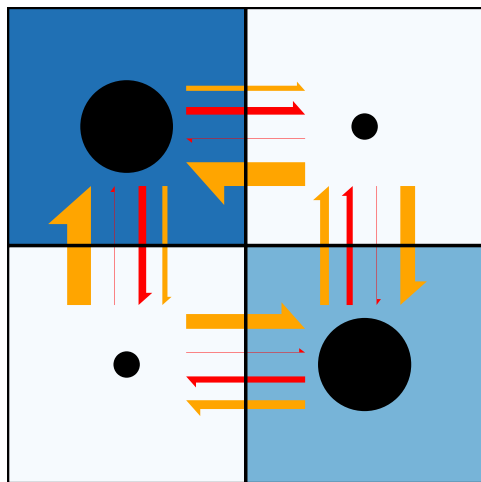
⁶These are the best solutions found by the model, which may or may not be the global optima due to non-convexity.



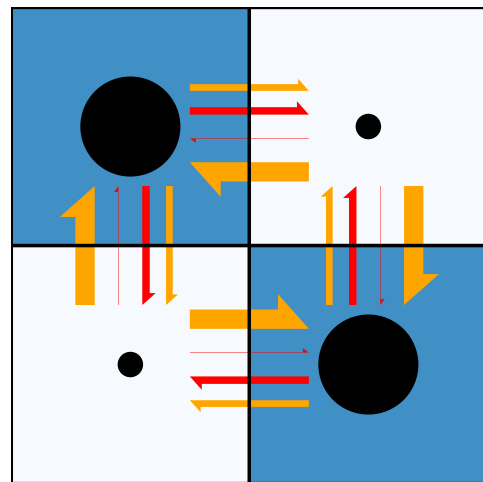
(a) Study region with four zones.



(b) Scenario S1.



(c) Scenario S2.



(d) Scenario S3.

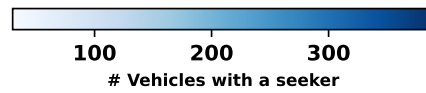
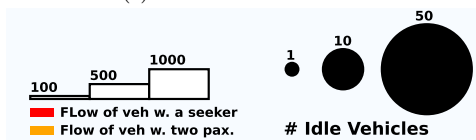


Figure 5: The hypothetical study region, and illustration of idle vehicle count, seeker vehicle count, and cross-zone vehicle flow in scenarios S1-S3.

zones 1, 2, and 4 have the same demand rates, zone 2 has more idle vehicles than the other two. This difference highlights the impact of ride-sharing — since zone 2 is diagonally positioned to zone 3, passengers going from zone 1 (or zone 4) to zone 3 can take advantage of the “passing” vehicles going from zone 2 towards zone 3. Hence, zone 1 and zone 4 require fewer idle vehicles than zone 2. From Figure 5b, we see that the vehicles with a seeker are distributed similarly in the four zones; i.e., zone 3 has far more vehicles with a seeker than zones 1, 2, and 4.

It is also interesting to observe that the travel directions of vehicles crossing neighboring zones are optimized as well. In Figure 5b, the flow of vehicles that carry a seeker out of zones 1, 2, and 4 is very small, possibly because most of these zones’ inter-zonal passengers are going to zone 3, and hence it is likely that they will match up with each other before they leave their zone (i.e., only few of them leave their zone as a seeker). On the contrary, since the trip rate from zone 3 to zones 1, 2, and 4 is relatively low, the probability to match two inter-zonal passengers inside zone 3 is relatively low, and in turn, many of them leave zone 3 as a seeker. For the vehicle travel path decisions, by symmetry between zone 1 and zone 4, about half of the seekers going between zone 2 and zone 3 should be routed through zone 1 or zone 4; i.e., $\delta_{23.1} = 0.54$, $\delta_{23.4} = 0.46$, $\delta_{32.1} = \delta_{32.4} = 0.50$. However, this is not the case for the seekers going between zone 1 and zone 4 (e.g., $\delta_{14.2} = \delta_{41.2} = 1.00$, $\delta_{14.3} = \delta_{41.3} = 0.00$), because zone 3 is the major destination zone with many idle vehicles and seekers inside, and hence it is beneficial to route all seekers going between zone 1 and zone 4 through zone 2 so as to better serve the passengers there.

In Scenario S2, a second, yet smaller, CBD emerges in zone 2 and diverts some of the trips away from zone 3. It is expected that more idle vehicle are now observed in zone 2, as more delivery trips end there. Interestingly, the number of idle vehicles in zone 3 also increases (as compared to Scenario S1), even though fewer vehicles now enter zone 3 to deliver passengers. A possible explanation is that the number of vehicles with a seeker has also decreased in zone 3 (e.g., by comparing the background color of zone 2 in Figures 5c and 5b), and this increases its needs for idle vehicles. In the meantime, the numbers of idle vehicles in zone 1 and zone 4 both decrease, possibly because a more even trip distribution between zone 2 and zone 3 increases the probability to match passengers going between zone 1 and zone 4 with seekers going between zone 2 and zone 3. Correspondingly, there is a smaller flow of vehicles with a seeker leaving zone 1 and zone 4, but a larger flow leaving zone 2; the reason could be that the lower demand into zone 3 reduces the probability for two inter-zonal passengers to be matched inside zone 2.

As the CBD in zone 2 continues to grow and eventually becomes symmetrical to that in zone 3, as in Scenario S3, the trend of changes in vehicle distribution agrees with that observed in Scenario S2. Moreover, the numbers of idle vehicles in zone 2 and zone 3 are now the same, as expected. The values of $\delta_{14.2}$, $\delta_{14.3}$, $\delta_{41.2}$, and $\delta_{41.3}$ are not reported in Table 1 because the corresponding flow of vehicles with a seeker out of zones 1 and 4 now is negligible, and hence the corresponding vehicle travel directions have no impacts on the system performance.

Table 1 also shows that, as demand distribution goes from monocentric (S1) to bicentric (S3), the total number of active vehicles increases but the number of rebalanced vehicles decreases. This is reasonable too. The trip destinations are spatially highly unbalanced in the monocentric scenario, which imposes a huge burden on vehicle rebalancing activities. However, in the meantime, since the trip destinations are concentrated in zone 3, the passenger matching probability is high and the ride-sharing service can be operated efficiently. As the trip destinations become more “scattered” in the bicentric scenario, the matching probability decreases, while the rebalancing operation is reduced as well. Overall, we see that the optimal total fleet needed in the entire region, M , changes

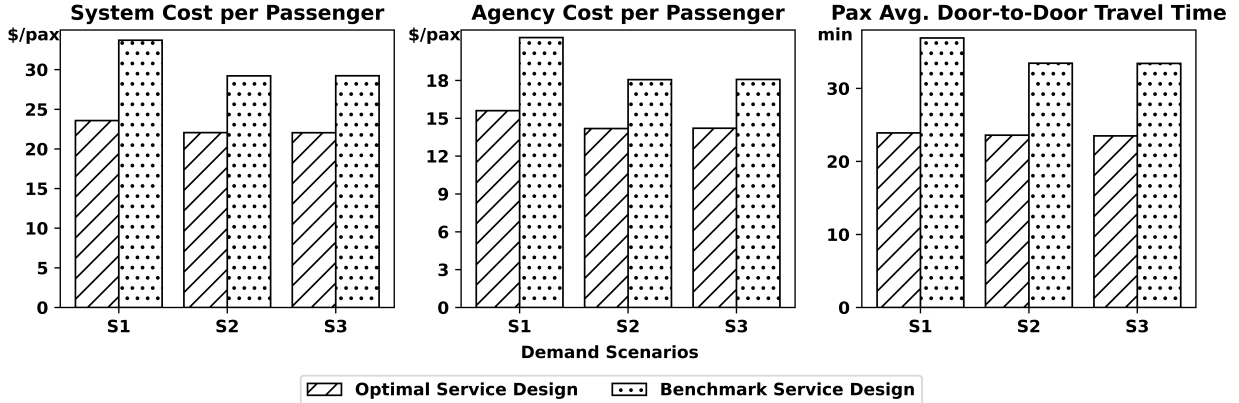


Figure 6: Comparisons of system performance under optimal service design and benchmark service design.

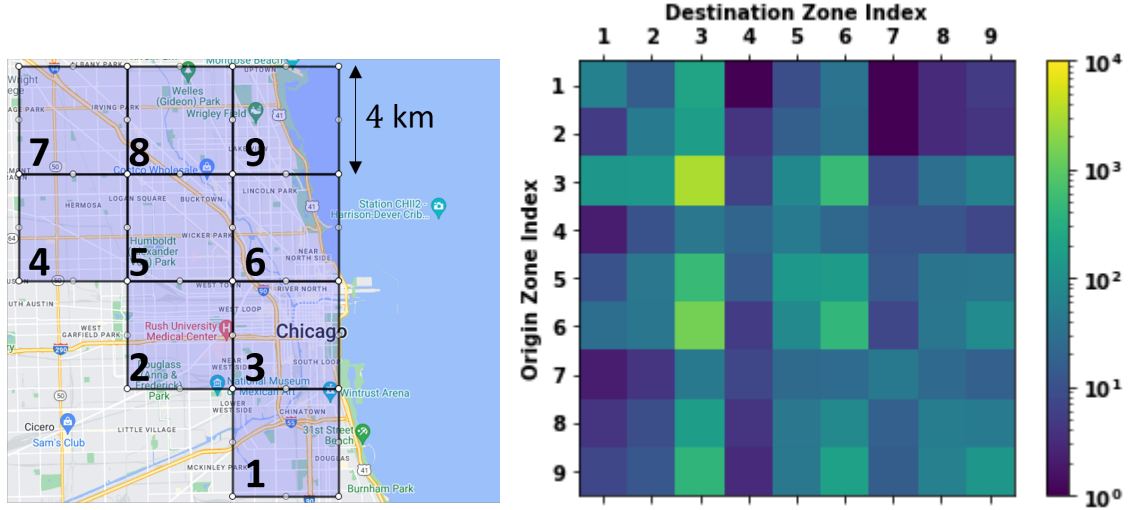
from 2401 in Scenario S1, to 2183 in Scenario S2, and to 2187 in Scenario S3. Correspondingly, the optimal system performance for the three demand scenarios, measured in terms of average system cost Z , agency cost per passenger $\gamma M / (\sum \lambda_{ij})$, and passenger door-to-door travel time $P / (\sum \lambda_{ij})$, are illustrated in Figure 6. The average system cost decreases from S1 to S3, and the majority of the saving comes from reduced agency cost, especially from reduced rebalancing vehicles. The average passenger door-to-door travel time also decreases, but only slightly.

To highlight the importance of capturing demand heterogeneity in service design, we consider a benchmark service design that assumes homogeneously distributed demand $\lambda_{ij} = 500$ trip/hr $\forall i, j$, with the total demand rate remains 8,000 trip/hr. The optimal solution for this homogeneous demand scenario is: $n_{1000} \approx n_{2000} \approx n_{3000} \approx n_{4000} \approx 0.11$ and $\delta_{14.2} = 0.26$, $\delta_{14.3} = 0.74$, $\delta_{41.2} = 0.44$, $\delta_{41.3} = 0.56$, $\delta_{23.1} = 0.48$, $\delta_{23.4} = 0.52$, $\delta_{32.1} = 0.49$, $\delta_{32.4} = 0.51$. We next implement this benchmark design into Scenarios S1-S3, and evaluate its performance under these heterogeneous demand patterns. The results are also plotted in Figure 6 for comparison. As compared to the benchmark service design, the optimal service design can reduce system-wide cost by 24.51% \sim 30.01%, agency cost by 21.38% \sim 27.08%, and passenger travel time by 29.45% \sim 35.23%. The differences in all these system performance metrics are quite significant. Hence, failure to address demand heterogeneity could lead to notably suboptimal service designs.

3.2. Chicago Case Study

In this section, we apply the proposed model to a subarea of Chicago, which is partitioned into 9 zones with $\Phi = 4$ km, as shown in Figure 7a. We extract TNC and taxi trip data for the morning rush (7:00 AM \sim 9:00 AM) in the entire year of 2019 from the Chicago Data Portal (City of Chicago, 2019a,b), and aggregate them into hourly zone-to-zone trip rates; see Figure 7b. The total trip rate for the entire study region is 9,520 trips per hour. The trips from and to those zones along the downtown and lake shore areas (e.g., zone 3, 6, 5, and 9) are orders of magnitude greater than those for others; e.g., the hourly incoming trip rate is 6,196 trip/hr for zone 3, but only 64 trip/hr for zone 4. Because the 2019 data may not be exhaustive, and because the TNC service is growing very rapidly, we follow Lei et al. (2020) and consider scaling all trip rates by a common factor $q \geq 1$.

We solve the optimal service design and system performance while varying the passenger value-of-time $\beta \in \{10, 20, 30\}$ \$/hr and the demand scaling factor $q \in \{1, 2, 3\}$. All other parameters are



(a) Partition of the study region.

(b) Trip Generation Rates of Zone-level OD $\{\lambda_{ij}\}$.

Figure 7: Zone partition and taxi/TNC trip OD matrix of the Chicago case study.

q	β	n_{1000}	n_{2000}	n_{3000}	n_{4000}	n_{5000}	n_{6000}	n_{7000}	n_{8000}	n_{9000}	$\sum_i M_i$	M_b	M
1	10	4	0	41	2	5	2	1	2	4	1847	257	2104
	20	7	0	67	3	7	2	2	3	4	1873	252	2125
	30	7	2	91	4	10	2	3	4	6	1901	252	2154
2	10	6	0	74	3	6	3	2	3	5	3570	519	4089
	20	11	0	123	4	8	3	3	4	6	3618	506	4124
	30	14	0	171	5	12	3	5	5	7	3672	499	4172
3	10	7	0	106	3	7	4	2	4	6	5262	785	6047
	20	14	0	180	5	9	4	4	4	7	5334	763	6097
	30	20	0	249	6	11	3	6	6	8	5410	750	6160

Table 2: Optimal design for the Chicago study region under varying q and β .

the same as those in the hypothetical example.

Table 2 summarizes the optimal number of idle vehicles in each zone for all combinations of q and β . When $q = 1$ and $\beta = 10$ \$/hr, the deployment of idle vehicles generally follows the demand distribution, as expected; e.g., zones 3, 5 and 9 have larger numbers, and zones 4 and 7 have smaller numbers. However, it is interesting to observe some exceptions. For example, zone 1 has the third largest number of idle vehicles, although its demand is relatively low. This discrepancy reflects the joint impacts of geometry and ride-sharing — no vehicles from other zones would pass zone 1 on their delivery routes, and hence the service in zone 1 heavily relies on the idle vehicles inside. On the contrary, zones 2 and 6 have very few (or even no) idle vehicles to serve their notable number of trips, mainly because these two zones are between high-demand zone 3 and all northern and western zones (i.e., zones 4, 5, 7, 8, and 9), and hence the passengers in zones 2 and 6 can be

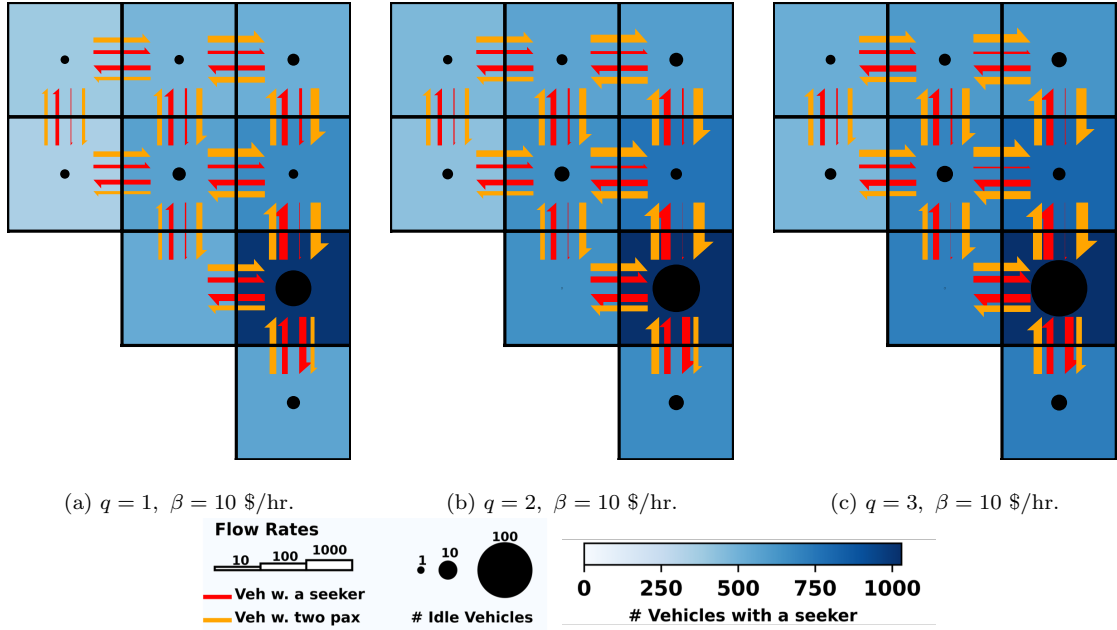


Figure 8: Illustration of idle vehicle count, seeker vehicle count, and cross-zone vehicle flow for the Chicago case study.

served by passing vehicles. These observations are consistent with the flow of vehicles (especially those with a seeker) in Figure 8a.

As q increases, it is noted from Table 2 that the number of idle vehicles in high-demand zone 3 increases almost linearly with q . It is possible that even when $q = 1$, passengers in zone 3 are well matched and ride-sharing opportunities have been fully utilized. Therefore, when demand increases, the number of idle vehicles in zone 3 must also increase. On the other hand, the idle vehicle counts in low-demand zones increase only mildly (or do not increase at all), probably because these zones can still benefit from a higher matching probability under higher demand. Overall, both the total number of active vehicles and that of rebalanced vehicles increase with q , almost proportionally, since there are more trips to serve and the absolute unevenness in demand distribution becomes more severe. More information about the vehicle counts and the flow between neighboring zones are visualized in Figure 8. For all zones, the numbers of vehicles increase with q . The vehicle flow also generally increases, except for a few exceptions (e.g., those with a seeker, going from zone 8 to zone 5, from zone 9 to zone 6, and from zone 6 to zone 3) due to simultaneous changes in the matching probabilities (similar to the observation from the hypothetical cases).

As β increases, the system tends to emphasize more on passenger experience, and hence it is reasonable to observe (slightly) more idle vehicles for almost every zone. As a whole, the total number of active vehicles also increases, but only moderately, and almost all the increases come from idle vehicles – as these vehicles most directly contribute to enhancement of passenger experience. Similarly, when the demand remains the same, the increasing value of β does not affect the total number of rebalanced vehicles significantly, as expected.

Figure 9 illustrates how the optimal system performance varies with q and β . A larger value of q always yields a lower average system cost, average agency cost, and average passenger travel time; this exhibits economies of scale, as expected. Given q , the average passenger travel time decreases

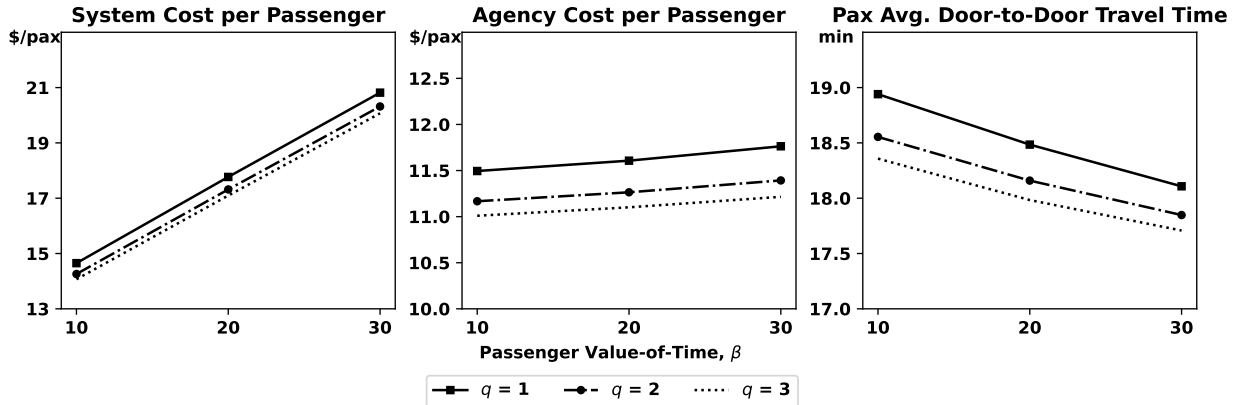


Figure 9: System performance under optimal design under varying q and β .

with β , while the agency cost increases — overall, the average system-wide cost increases.

4. Conclusion

This paper proposed a multi-zone queuing network model to describe how TNCs shall plan ride-sharing services for areas with spatially heterogeneous demand. The model incorporates TNC’s decisions, including deployment of vehicles in each zone, vehicle travel directions between zones, and the rate to rebalance vehicles between zones. A set of criteria are imposed to avoid excessive detours for matched passengers. The steady-state operation of the ride-sharing service is modeled by a multi-zone aspatial queuing network, composed of a set of vehicle states that describe vehicles’ location and workload, and a set of flow variables that describe vehicles’ transitions within and across zones. A large system of nonlinear equations is formulated based on the queuing network model, and its solution can be used to evaluate the expected system-wide cost in the steady state. The design of ride-sharing services is optimized as a constrained nonlinear program. A customized solution approach is proposed to decompose and solve the optimization problem.

The proposed model and solution approach are tested through a series of hypothetical examples and a real-world case study. The results reveal interesting insights into the optimal service design characteristics; e.g., how idle vehicles and partially-occupied vehicles complement each other in providing services, how the need for vehicles in a zone depends on not only its own travel demand but also those in other zones, and how important it is to properly address demand heterogeneity when designing ride-sharing services.

The work in this paper can be extended in multiple directions. First, this paper assumes a certain type of ride-sharing service. However, many other demand-responsive services (e.g., taxi service, dial-a-ride) could be considered as well, because they can be modeled under a similar queuing network model (Daganzo and Ouyang, 2019a). In addition, although ride-sharing service is advantageous for high-demand areas (such that the matching probability is high), it may be beneficial to use non-shared taxi service where demand is very low. Therefore, an interesting extension to this paper is to allow the TNC platform to decide which zones to provide which type of service, or which combinations of services, and how the TNCs can optimally set the prices for different services (see similar efforts in Zhang and Nie (2021) and Jacob and Roet-Green (2021)). In this paper, demand is spatially heterogeneous but temporally homogeneous. In the real world,

demand is often also notably heterogeneous in the time dimension; it would be interesting to explore the system dynamics based on either continuous (e.g., the fluid model in Xu et al. (2021b)) or discrete models (e.g., cell transmission model in Daganzo (1994) and zone-based system in Lei et al. (2020)). Finally, this paper assumes constant vehicle speed. In future research, it is possible to consider local traffic congestion as a function of the number of vehicles in each zone (e.g., using a macroscopic fundamental diagram as in Daganzo and Geroliminis (2008)), and quantify the travel time of vehicles and passengers under explicit consideration of traffic delay. In so doing, we can also incorporate environmental impacts and externalities into the service design model.

Appendix A. List of Key Notation

See Table 3 for the list of key notation defined in this paper.

Notation	Description
Indices and Sets	
\mathcal{K}	Set of all zones in the study region, indexed by i, j, k .
G_i^r	Set of zones in the r direction of zone i .
\mathcal{V}_{ij}	Set of zones that a vehicle going to zone j can enter upon leaving zone i .
U^r	Set of two directions adjacent to direction r .
$\Omega_{ii}^r, \Omega_{ij}^r$	Sets of zones in the destination feasible areas for a caller going in the r direction within zone i and a caller going from zone i to zone j , respectively.
A_i^r	Index of the adjacent zone on the r side of zone i .
$s = (s_0, s_1, s_2, s_3)$	Vehicle state vector, s_0 – vehicle current zone, s_1 – assigned caller’s origin zone, s_2 and s_3 – onboard passengers’ destination zones.
Parameters	
Φ [km]	Side length of the square local zone.
v [km/hr]	Travel speed of ride-sharing vehicles.
γ [\$/hr]	TNC vehicle operation cost.
β [\$/hr]	Passenger value-of-time.
λ_{ij} [trip/hr]	Generation rates of trips from zone i to zone j .
L_{ij} [km]	Shortest distance between zone centroids on road network.
Variables	
a, p, d, c, g, b [veh/hr]	Vehicle state transition rates due to assignment, pickup, delivery, crossing a zone boundary, or rebalancing between zones.
n_s	Number of vehicles in state s .
$\delta_{ij-i'}$	% of vehicles going to zone j that enter zone i' upon leaving zone i .
N_{ii}^r, N_{ij}^r	Numbers of suitable vehicles to serve a caller going in the r direction within zone i and to serve a passenger going from zone i to zone j , respectively.
M_i, M_b, M [veh-hr/hr]	Vehicle hours in operation for active vehicles in zone i , rebalanced vehicles, and all vehicles in the system, respectively.
P [pax-hr/hr]	Total trip time spent by all passengers per hour.
Z [\$/pax]	System-wide cost per passenger.

Table 3: Key notation in this paper.

Appendix B. Expected Passenger-Vehicle Matching, and Proofs of Eqn. (7)-(9)

In this appendix, we derive formulas to show how the assignment rates and pickup rates are related to the number of vehicles in each state, as in Eqn. (7)–(9), according to the assignment policy and matching criteria.

Recall that any caller in zone i may be served by an idle vehicle in state $(i, 0, 0, 0)$, or a vehicle in state $(i, 0, i, 0)$ (i.e., with a seeker destined in zone i), or a vehicle in state $(i, 0, j, 0)$ (i.e., with a seeker destined in another zone j). Based on the matching criteria, all n_{i000} idle vehicles are

suitable to serve any caller, but only a portion of vehicles in states $(i, 0, i, 0)$ or $(i, 0, j, 0)$ can be suitable.

If an intra-zonal caller is going, say, in the NE direction, the destination feasible area for seekers in state- $(i, 0, i, 0)$ vehicles is indicated by Figure 2a, and the expected size of this feasible area is $2/9$ of the zone.⁷ Therefore, the expected number of suitable state- $(i, 0, i, 0)$ vehicles is $2n_{i0i0}/9$. A state- $(i, 0, j, 0)$ vehicle is suitable if its seeker's destination is in a zone of Ω_{ii}^{NE} , as shown in Figure 3a; therefore, the number of suitable state- $(i, 0, j, 0)$ vehicles is $\sum_{j \in \Omega_{ii}^{\text{NE}}} n_{i0j0}$. Then, the total number of suitable vehicles for an intra-zonal caller going in the NE direction, N_{ii}^{NE} , is as follows,

$$N_{ii}^r = n_{i000} + \frac{2n_{i0i0}}{9} + \sum_{j \in \Omega_{ii}^r} n_{i0j0}, \quad \forall i \in \mathcal{K}, r \in \{\text{NE}\}.$$

By symmetry, the above formula holds for any travel direction $r \in \{\text{NE}, \text{NW}, \text{SW}, \text{SE}\}$, which yields Eqn. (7).

When the caller is inter-zonal, e.g., going from zone i to zone j , we can obtain the number of suitable vehicles in a similar way. Among the seekers in state- $(i, 0, i, 0)$ vehicles, we expect $1/2$ of them to have their destinations aligned with that of the inter-zonal caller if $j \in G_i^{\text{S}}$ (e.g., see the blue shaded area in Figure 3b), or $1/4$ if $j \in G_i^{\text{NE}}$ (e.g., see the red shaded area in Figure 3b). Among the state- $(i, 0, k, 0)$ vehicles, they are suitable if their seekers' destination zones are in Ω_{ij} (e.g., see the shaded area in Figure 2b). Hence, the number of suitable vehicles for an inter-zonal caller going from zone i to zone j , N_{ij} , is as follows,

$$\begin{aligned} N_{ij} &= n_{i000} + \frac{n_{i0i0}}{4} + \sum_{k \in \Omega_{ij}} n_{i0k0}, & \forall i \in \mathcal{K}, j \in G_i^r, r \in \{\text{NE}\} \\ N_{ij} &= n_{i000} + \frac{n_{i0i0}}{2} + \sum_{k \in \Omega_{ij}} n_{i0k0}, & \forall i \in \mathcal{K}, j \in G_i^r, r \in \{\text{S}\}. \end{aligned}$$

Again, by directional symmetry, we can see that Eqn. (8) holds.

Now we determine the caller pickup rates in Eqn. (9). Since the TNC always assigns the nearest suitable vehicle to a caller, and the vehicles in each state are approximately uniformly distributed in a zone, the probability for a caller to be assigned to a vehicle in state s is proportional to the relative density of that type of vehicles. Also, the rate for vehicles in state s to be assigned to a type of callers should be equal to the rate for vehicles in state s to pick up that type of callers. Therefore, we can determine the pickup rates based on all types of suitable vehicles, n_{i000} , n_{i0i0} , $\{n_{i0j0}\}_{j \neq i}$.

For example, in zone i , symmetry indicates that intra-zonal callers going in the $r \in \{\text{NE}, \text{NW}, \text{SW}, \text{SE}\}$ direction are generated at rate $\lambda_{ii}/4$, and a fraction of n_{i000}/N_{ii}^r of them are picked up by an idle vehicle. Therefore, the rate for idle vehicles to pick up intra-zonal callers, $p_{ii00.i}$, can be obtained by summing the product of these two quantities, $(\lambda_{ii}/4) \cdot (n_{i000}/N_{ii}^r)$, across all four directions; i.e.,

$$p_{ii00.i} = \sum_{r \in \{\text{NE}, \text{NW}, \text{SW}, \text{SE}\}} \left(\frac{\lambda_{ii}}{4} \cdot \frac{n_{i000}}{N_{ii}^r} \right).$$

⁷Recall that the callers' ODs are homogeneously distributed within the zone; readers can refer to Appendix 7B of Daganzo and Ouyang (2019b) for the derivation of this quantity.

This gives Eqn. (9.1). The rate for state- $(i, 0, i, 0)$ vehicles to pick up intra-zonal callers, $p_{iii0.i}$, can be derived similarly, except that the number of suitable state- $(i, 0, i, 0)$ vehicles is $2n_{i0i0}/9$ instead of n_{i000} ; i.e.,

$$p_{iii0.i} = \sum_{r \in \{\text{NE, NW, SW, SE}\}} \left(\frac{\lambda_{ii}}{4} \cdot \frac{2n_{i0i0}}{9N_{ii}^r} \right).$$

This gives Eqn. (9.2). Per the matching criterion in Case 3, an intra-zonal caller going in the $r \in \{\text{NE, NW, SW, SE}\}$ direction can also be picked up by a state- $(i, 0, j, 0)$ vehicle, whose seeker is either (i) going to a zone j in the exact same direction r (i.e., $j \in G_i^r$); or (ii) going to a zone j in an adjacent direction (i.e., $j \in G_i^{r'}, \forall r' \in U^r$). Conversely, from the vehicle's point of view, a state- $(i, 0, j, 0)$ vehicle with a seeker going to a zone on the $r \in \{\text{NE, NW, SW, SE}\}$ direction can only serve an intra-zonal passenger of the exact same direction; the rate for pickup is

$$p_{ij0.i} = \frac{\lambda_{ii}}{4} \cdot \frac{n_{i0j0}}{N_{ii}^r}, \quad \forall i \in \mathcal{K}, j \in G_i^r, r \in \{\text{NW, SW, SE, NE}\}.$$

This gives Eqn. (9.3). Yet, a state- $(i, 0, j, 0)$ vehicle with a seeker going in a direction $r' \in \{\text{E, N, W, S}\}$ can serve intra-zonal passengers that are going in the two adjacent directions of r' , as given by $U^{r'}$; i.e.,

$$p_{ij0.i} = \sum_{r \in U^{r'}} \left(\frac{\lambda_{ii}}{4} \cdot \frac{n_{i0j0}}{N_{ii}^r} \right), \quad \forall i \in \mathcal{K}, j \in G_i^{r'}, r' \in \{\text{N, W, S, E}\}.$$

This gives Eqn. (9.4).

When a caller is inter-zonal with its destination in zone j , the analysis is similar. We only need to note that the trip rate is now λ_{ij} , and the total number of suitable vehicles is now N_{ij} . The reader is encouraged to verify that the pickup rates for inter-zonal callers by different types of vehicles, as counterparts of those for intra-zonal callers, are given by Eqn. (9.5)-(9.8).

Appendix C. Expected State Duration, and Proofs of Eqn. (10)-(11)

This appendix derives the expected vehicle travel distance in each state, first among the ‘‘assigned’’ and rebalancing states, and then the ‘‘delivery’’ states. These distances will be used to quantify the rates at which vehicles finish passenger delivery within zone i , as in Eqn. (10), and to obtain the count of vehicles in each state, as in Eqn. (11).

Appendix C.1. Assigned and rebalancing state duration

In zone i , a vehicle is en-route to pick up an assigned passenger if it is in state $(i, i, 0, 0)$, $(i, i, i, 0)$, and $(i, i, j, 0)$, $\forall j \in \mathcal{K} \setminus \{i\}$. The expected pickup travel distance under the nearest vehicle assignment rule, per discussion in Daganzo and Ouyang (2019b), is simply inversely proportional to the number of suitable vehicles; i.e., $0.63\Phi/\sqrt{N_{ii}^r}$ if the passenger is intra-zonal and going in the $r \in \{\text{NE, NW, SW, SE}\}$ direction, or $0.63\Phi/\sqrt{N_{ij}}$ if the passenger is inter-zonal and going to zone $j \in \mathcal{K} \setminus \{i\}$. Dividing these distances by the vehicle speed v yields the expected trip durations. Therefore, by Little's Law (Little, 1961), the vehicle count in state $(i, i, 0, 0)$ can be obtained by summing the product of each expected trip duration, $\frac{0.63\Phi}{v\sqrt{N_{ii}^r}}$ or $\frac{0.63\Phi}{v\sqrt{N_{ij}}}$, and the corresponding pickup

rate, $\frac{\lambda_{ii} n_{i000}}{4 N_{ii}^r}$ from Eqn. (9.1) or $\lambda_{ij} \frac{n_{i000}}{N_{ij}}$ from Eqn.(9.5), across all intra-zonal travel directions $r \in \{\text{NE, NW, SW, SE}\}$ and all inter-zonal passenger destination zones $j \in \mathcal{K} \setminus \{i\}$. The result leads to Eqn.(11.1).

The vehicle counts in states $(i, i, i, 0)$ and $(i, i, j, 0)$ shall be similar, except that (i) the rates for state- $(i, i, i, 0)$ vehicles and state- $(i, i, j, 0)$ vehicles to pick up an intra-zonal passenger are given by Eqn. (9.2) and Eqn. (9.3)-(9.4), respectively; and (ii) the rates for state- $(i, i, i, 0)$ vehicles and state- $(i, i, j, 0)$ vehicles to pick up an inter-zonal passenger are given by Eqn. (9.6)-(9.7) and Eqn. (9.8), respectively. The readers can then verify from Little's formula that the vehicle counts in these two states are given by Eqn. (11.2)-(11.4).

Finally, it shall be clear that the expected travel distance for a vehicle to be rebalanced from a random point in zone i to a random point in zone j shall be equal to the distance between the zone centroids, L_{ij} , if these two zones are not horizontally or vertically aligned (i.e., $j \in G_i^r$ with $r \in \{\text{NE, NW, SW, SE}\}$). Otherwise, if $j \in G_i^r$ with $r \in \{\text{E, N, W, S}\}$, we need to add an additional "lateral" travel distance that is equal to one third of the zone width (Daganzo and Ouyang, 2019b); i.e., the expected distance becomes $L_{ij} + \frac{\Phi}{3}$. Little's formula then leads to Eqn. (11.8)-(11.9).

Appendix C.2. Delivery state duration

In zone i , a vehicle is en-route to drop off an onboard passenger if it is in state $(i, 0, i, 0)$, $(i, 0, i, i)$, $(i, 0, j, 0)$, $(i, 0, i, j)$ or $(i, 0, j, k)$, $\forall j \in \mathcal{K} \setminus \{i\}$, $k \in \tilde{\Omega}_{ij}$. The expected travel distances for vehicles in these states are more complicated, because these vehicles may have one or two onboard passenger(s) who could be intra-zonal or inter-zonal, and these vehicles may transition into and out of the current state due to multiple types of events: picking up or delivering a passenger, receiving a new assignment, and crossing the zone boundary.

For example, as Figure 4 shows, a state- $(i, 0, i, i)$ vehicle could have transitioned from either state $(i, i, i, 0)$, at rate $p_{iii0.i}$, or state $(i', 0, i, i)$ (where $i' \in \{A_i^E, A_i^N, A_i^W, A_i^S\}$), at rate c_{i0ii} .

In the former case, the delivery trip starts upon picking up the recently assigned caller at its origin (a random location, denoted P0), and ends upon delivering the onboard passenger with a closer destination. Since these two passengers are both intra-zonal, to avoid any detours (as required by the matching criterion in Case 1), the two passenger destinations (denoted P1, P2) must be aligned, and the first delivery destination must be closer to P0. We use (x_0, y_0) , (x_1, y_1) , and (x_2, y_2) to represent the Cartesian coordinates of P0, P1, and P2, respectively. Figure C.10a shows an example where P1 and P2 are located in the NE direction of P0 (i.e., $x_1, x_2 \geq x_0$ and $y_1, y_2 \geq y_0$). The distance of the first delivery trip is clearly

$$\min\{x_1, x_2\} - x_0 + \min\{y_1, y_2\} - y_0. \quad (\text{C.1})$$

As $x_0, x_1, x_2, y_0, y_1, y_2$, are each independently and uniformly distributed in $[0, \Phi]$, we see that

$$\mathbb{E}[x_1 - x_0 | x_0 \leq x_1 \leq x_2] = \int_0^\Phi \int_{x_0}^\Phi \int_{x_0}^{x_2} \frac{x_1 - x_0}{\Phi(\Phi - x_0)(x_2 - x_0)} dx_1 dx_2 dx_0 = \frac{\Phi}{8}.$$

Then, by symmetry between x_1 and x_2 , we see that

$$\mathbb{E}[\min\{x_1, x_2\} - x_0 | x_1, x_2 \geq x_0] = \mathbb{E}[x_1 - x_0 | x_0 \leq x_1 \leq x_2] + \mathbb{E}[x_2 - x_0 | x_0 \leq x_2 \leq x_1] = \frac{\Phi}{4}.$$

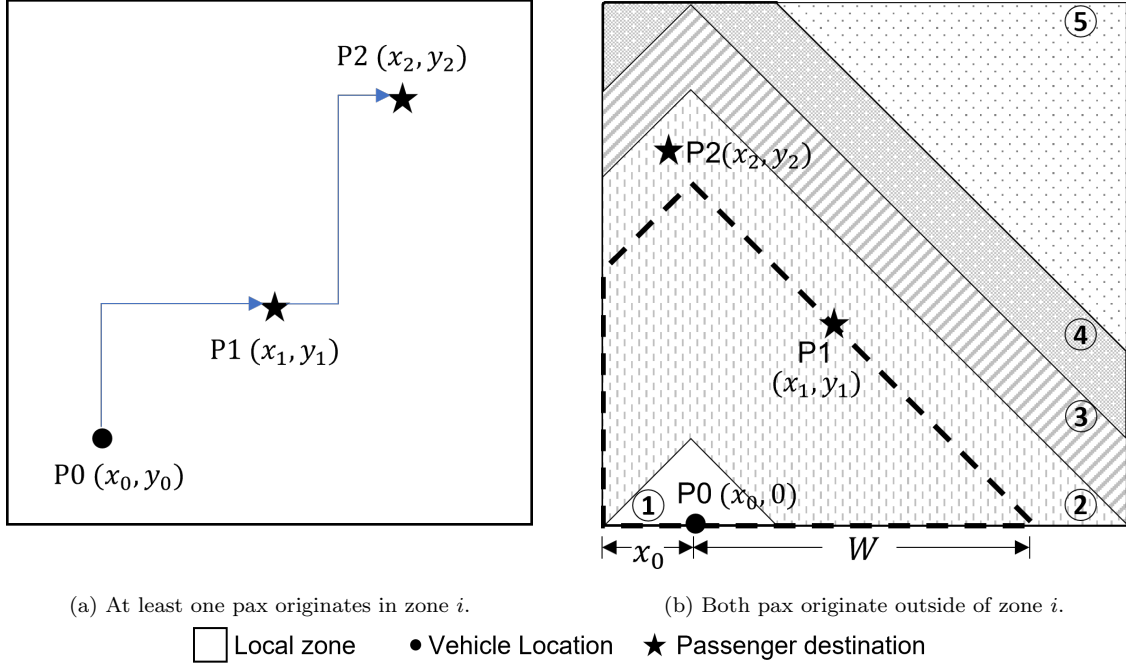


Figure C.10: Trip for a state- $(i, 0, i, i)$ vehicle to deliver two onboard passengers inside a zone.

The symmetry between x - and y -coordinates further tells us that the expectation of (C.1) is $2 \cdot \frac{\Phi}{4} = \frac{\Phi}{2}$. This expectation clearly does not depend on the exact direction of travel. Upon completing the first delivery trip, the vehicle transitions into state $(i, 0, i, 0)$ and starts to deliver the second passenger. Symmetry implies that the expected distance of the second delivery trip, e.g., $|x_2 - x_1| + |y_2 - y_1|$ in Figure C.10a, also equals $\frac{\Phi}{2}$.⁸

In the latter case, the delivery trip in state $(i, 0, i, i)$ starts when the vehicle first enters zone i at a random point $P0$ on the boundary; as illustrated in Figure C.10b. By matching criterion Case 2, detour within zone i is allowed when delivering two such inter-zonal passengers, and the delivery sequence is strictly based on the distances from $P0$ to the two onboard passengers' destinations $P1$ and $P2$. The length of the first delivery trip, $\min\{|x_1 - x_0| + |y_1 - 0|, |x_2 - x_0| + |y_2 - 0|\}$, cannot be simplified to Eqn. (C.1) as in the former case, since $P1$ and $P2$ are two random points in this case. Let W denote the first delivery trip length, and since it depends on the x -coordinate of $P0$, x_0 , we can obtain its expectation by first calculating the conditional expectation on x_0 , as follows:

$$\mathbb{E}[W] = \mathbb{E}[\mathbb{E}[W|x_0 = x]] = \frac{1}{\Phi} \int_0^{\Phi} \int_0^{2\Phi-x} \bar{F}_{W|x_0}(w|x) dw dx.$$

Here $\bar{F}_{W|x_0}(w|x)$ is the complementary cumulative distribution function of W conditional on x_0 , which equals the conditional probability that both $P1$ and $P2$ are outside of the dashed polygon in Figure C.10b). Simple geometry shows that $\bar{F}_{W|x_0}(w|x)$ is a piece-wise function, and when $x \leq \frac{\Phi}{2}$, it satisfies the following,

⁸As such, the expected delivery distance of a state- $(i, 0, i, 0)$ vehicle is $\frac{\Phi}{2}$ if this vehicle comes from state $(i, 0, i, i)$ and it previously enters state $(i, 0, i, i)$ via a passenger pickup (which occurs at rate $p_{iii0.i}$).

$$\bar{F}_{W|x_0}(w|x) = \begin{cases} \left(1 - \frac{w^2}{\Phi^2}\right)^2, & \text{if } w \leq x \\ \left(1 - \frac{w^2 + 2xw - x^2}{2\Phi^2}\right)^2, & \text{if } x \leq w \leq \Phi - x \\ \left(1 - \frac{2\Phi w + 2\Phi x - 2x^2 - \Phi^2}{2\Phi^2}\right)^2, & \text{if } \Phi - x \leq w \leq \Phi \\ \left(1 - \frac{6\Phi w + 2\Phi x - 2x^2 - 3\Phi^2 - 2w^2}{2\Phi^2}\right)^2, & \text{if } \Phi \leq w \leq \Phi + x \\ \left(1 - \frac{(2\Phi - w - x)^2}{2\Phi^2}\right)^2, & \text{if } \Phi + x \leq w \leq 2\Phi - x. \end{cases}$$

These five cases correspond to areas 1-5 in Figure C.10b, respectively. We first calculate $\mathbb{E}[W|x_0 \leq \frac{\Phi}{2}] = \frac{1}{\Phi/2} \int_0^{\Phi/2} \int_0^{2\Phi-x} \bar{F}_{W|x_0}(w|x) dw dx = \frac{5\Phi}{8}$. By symmetry, we know that $\mathbb{E}[W] = \frac{5\Phi}{8}$. Then, upon completing the first-delivery trip, the vehicle transitions into state $(i, 0, i, 0)$ to start the second delivery trip, which is between two random points P1 and P2 inside a square area of side Φ , so its expected distance is simply $\frac{2}{3}\Phi$ (Daganzo and Ouyang, 2019b).⁹

Similarly, we can estimate the travel distance of a vehicle in state $(i, 0, i, j)$. In this state, a vehicle drops off one of the onboard passengers whose destination is within zone i . This vehicle could have transitioned into the current state from (i) state $(i', 0, i, j)$ for $i' \in \{A_i^E, A_i^N, A_i^W, A_i^S\}$, at rate c_{i0ij} , and the delivery trip starts when the vehicle enters zone i at a random point on a zone boundary; (ii) state $(i, i, i, 0)$ (or $(i, i, j, 0)$) at rate p_{iii0j} (or p_{ijj0i}), and the delivery trip starts when the vehicle picks up an inter-zonal (or intra-zonal) passenger at a random location. In case (i), the expected travel distance is $\frac{5\Phi}{6}$, including the expected distance for the movement perpendicular to the zone boundary $\frac{\Phi}{2}$ and that for the movement parallel to the zone boundary $\frac{\Phi}{3}$. In case (ii), the expected travel distance is $\frac{2\Phi}{3}$. These results are summarized in Table 4.

In state $(i, 0, j, k)$, a vehicle could have transitioned into the current state by crossing the zone boundary, at rate c_{i0jk} ; then its trip shall start from a boundary point and pass through zone i to deliver the onboard passengers to other zones. Otherwise, the vehicle could have transitioned into the current state upon picking up an inter-zonal passenger (at a random interior location), at rate p_{ijj0k} ; then its trip shall start from the pickup location and end when it exits the zone boundary. Their expected distances are approximately Φ and $\frac{\Phi}{2}$, respectively. Again, these results are summarized in Table 4. By applying the Little's formula to these three states, $(i, 0, i, i)$, $(i, 0, i, j)$ and $(i, 0, j, k)$, we can obtain the formulas for their vehicle counts as given in Eqn. (11.5)-(11.7).

The analysis of a state- $(i, 0, i, 0)$ vehicle is similar but with a slight complication. This vehicle is en-route to deliver its only onboard seeker to its destination in zone i . As shown in Figure 4, this vehicle could have transitioned into the current state from (i) state $(i', 0, i, 0)$ for $i' \in \{A_i^E, A_i^N, A_i^W, A_i^S\}$, at inflow rate c_{i0i0} , upon entering zone i at a random boundary point; (ii) from state $(i, i, 0, 0)$, at inflow rate p_{ii00i} , upon picking up an assigned caller at a random interior point; or (iii) from state $(i, 0, i, i)$, at inflow rate d_{i0ii} , upon delivering one of its onboard passengers to the destination. In case (iii), this vehicle's delivery trip goes from the delivered passenger's destination to the remaining passenger's destination, and there are two possibilities: (iii-a) the two destinations can be two random points within zone i , if this vehicle enters state $(i, 0, i, i)$ by crossing zone boundary (at inflow rate c_{i0ii}); (iii-b) these two destinations impose no detour during

⁹Hence, the expected delivery distance for a state- $(i, 0, i, 0)$ vehicle is $\frac{2\Phi}{3}$ if this vehicle comes from state $(i, 0, i, i)$ and it previously enters state $(i, 0, i, i)$ by crossing the zone boundary (which occurs at rate c_{i0ii}).

State	Veh. Inflow	Exp. Dist.	Delivery Trip	
			Start	End
$(i, 0, i, i)$	c_{i0ii}	$\frac{5\Phi}{8}$	Random boundary point	Closer of two random interior points
	p_{iii0-i}	$\frac{\Phi}{2}$	Random interior point	Closer of two random interior points that impose no detour
$(i, 0, i, j)$	c_{i0ij}	$\frac{5\Phi}{6}$	Random boundary point	Random interior point
	p_{iii0-j}	$\frac{2\Phi}{3}$	Random interior point	Random interior point
	p_{ij0-i}	$\frac{2\Phi}{3}$	Random interior point	Random interior point
$(i, 0, j, k)$	c_{i0jk}	Φ	Random boundary point	Another boundary
	p_{ij0-k}	$\frac{\Phi}{2}$	Random interior point	A zone boundary (no lateral movement)
$(i, 0, i, 0)$	c_{i0i0}	$\frac{5\Phi}{6}$	Random boundary point	Random interior point
	p_{ii00-i}	$\frac{2\Phi}{3}$	Random interior point	Random interior point
	c_{i0ii}	$\frac{2\Phi}{3}$	Random interior point	Random interior point
	p_{iii0-i}	$\frac{\Phi}{2}$	Closer of two random interior points that impose no detour	Farther of two random interior points that impose no detour
$(i, 0, j, 0)$	c_{i0j0}	Φ	Random boundary point	Another boundary
	p_{ii00-j}	$\frac{\Phi}{2}$	Random interior point	A zone boundary (no lateral movement)
	d_{i0ij}	$\frac{\Phi}{2}$	Random interior point	A zone boundary (no lateral movement)

Table 4: Expected vehicle travel distance to deliver onboard passengers.

the delivery trip, if this vehicle enters state $(i, 0, i, i)$ by a recent pickup (at inflow rate p_{iii0-i}). This vehicle could end the current state when it completes the delivery of its current onboard passenger, which occurs at rate d_{i0i0} , or when a new caller is assigned to this vehicle before it finishes the delivery, which occurs at rate a_{i0i0} . If the vehicle does complete the delivery, as Table 4 summarizes, the expected vehicle travel distance in state $(i, 0, i, 0)$ is approximately $\frac{5\Phi}{6}$ for case (i); $\frac{2\Phi}{3}$ for case (ii); $\frac{2\Phi}{3}$ for case (iii-a), per footnote 9; or $\frac{\Phi}{2}$ for case (iii-b), per footnote 8. Yet, before the vehicle completes the delivery, a new caller assignment may arrive according to a Poisson Process with rate a_{i0i0}/n_{i0i0} (i.e., the total assignment rate a_{i0i0} is shared by n_{i0i0} vehicles in this state). Hence, the number of new assignments showing up to this vehicle during the delivery trip follows a Poisson distribution with mean $\frac{a_{i0i0}}{n_{i0i0}} \cdot \frac{5\Phi}{6v}$, $\frac{a_{i0i0}}{n_{i0i0}} \cdot \frac{2\Phi}{3v}$, $\frac{a_{i0i0}}{n_{i0i0}} \cdot \frac{2\Phi}{3v}$, and $\frac{a_{i0i0}}{n_{i0i0}} \cdot \frac{\Phi}{2v}$, for case (i), (ii), (iii-a) and (iii-b), respectively. As a result, the probability for the vehicle to successfully complete the delivery (without new assignment) is $\exp(-\frac{a_{i0i0}}{n_{i0i0}} \cdot \frac{5\Phi}{6v})$, $\exp(-\frac{a_{i0i0}}{n_{i0i0}} \cdot \frac{2\Phi}{3v})$, $\exp(-\frac{a_{i0i0}}{n_{i0i0}} \cdot \frac{2\Phi}{3v})$, and $\exp(-\frac{a_{i0i0}}{n_{i0i0}} \cdot \frac{\Phi}{2v})$, respectively. Therefore, the successful delivery rate d_{i0i0} shall be the weighted sum of all inflow rates c_{i0i0} , p_{ii00-i} , c_{i0ii} , and p_{iii0-i} , using their corresponding success probabilities as weights. This gives d_{i0i0} as in Eqn. (10.1).

The analysis of a state- $(i, 0, j, 0)$ vehicle is almost the same as that for a state- $(i, 0, i, 0)$ vehicle, except that it is now delivering an inter-zonal passenger. Figure 4 shows that this vehicle could have transitioned into the current state from state $(i', 0, j, 0)$ for $i' \in \{A_i^E, A_i^N, A_i^W, A_i^S\}$, at rate

c_{i0j0} (upon crossing a zone boundary); or from state $(i, i, 0, 0)$, at rate $p_{ii00..j}$ (upon picking up a recent inter-zonal caller from a random location); or from state $(i, 0, i, j)$, at rate d_{i0ij} (upon delivering an intra-zonal passenger at a random location). This vehicle state could end when this vehicle crosses the zone border, at rate g_{i0j0} , or when a new caller is assigned to this vehicle before it crosses the zone border, at rate a_{i0j0} . If no new assignment is ever received before the vehicle reaches a zone boundary, the corresponding expected travel distances are approximately Φ , $\frac{\Phi}{2}$, and $\frac{\Phi}{2}$, respectively, as summarized in Table 4. Note that new caller assignments arrive with rate a_{i0j0}/n_{i0j0} to this particular vehicle, then using a similar logic to that for calculating d_{i0i0} above, we can obtain the formula for g_{i0j0} as given in Eqn. (10.2).

References

- Affah, F., Guo, Z., 2022. Spatial pricing of ride-sourcing services in a congested transportation network. *Transportation Research Part C: Emerging Technologies* 142, 103777.
- Alisoltani, N., Leclercq, L., Zargayouna, M., 2021. Can dynamic ride-sharing reduce traffic congestion? *Transportation research part B: methodological* 145, 212–246.
- Alonso-Mora, J., Samaranayake, S., Wallar, A., Frazzoli, E., Rus, D., 2017. On-demand high-capacity ride-sharing via dynamic trip-vehicle assignment. *Proceedings of the National Academy of Sciences* 114, 462–467.
- Bei, X., Zhang, S., 2018. Algorithms for trip-vehicle assignment in ride-sharing, in: *Proceedings of the AAAI Conference on Artificial Intelligence*.
- Bimpikis, K., Candogan, O., Saban, D., 2019. Spatial pricing in ride-sharing networks. *Operations Research* 67, 744–769.
- Bynum, M.L., Hackebeil, G.A., Hart, W.E., Laird, C.D., Nicholson, B.L., Sirola, J.D., Watson, J.P., Woodruff, D.L., 2021. *Pyomo—optimization modeling in python*. volume 67. Third ed., Springer Science & Business Media.
- Caulfield, B., 2009. Estimating the environmental benefits of ride-sharing: A case study of dublin. *Transportation Research Part D: Transport and Environment* 14, 527–531.
- Chan, N.D., Shaheen, S.A., 2012. Ridesharing in north america: Past, present, and future. *Transport reviews* 32, 93–112.
- Chen, C., Yao, F., Mo, D., Zhu, J., Chen, X.M., 2021. Spatial-temporal pricing for ride-sourcing platform with reinforcement learning. *Transportation Research Part C: Emerging Technologies* 130, 103272.
- Chen, X., Chuqiao, C., Xie, W., 2019. Optimal spatial pricing for an on-demand ride-sourcing service platform. Available at SSRN 3464228 .
- Chen, X.M., Zahiri, M., Zhang, S., 2017. Understanding ridesplitting behavior of on-demand ride services: An ensemble learning approach. *Transportation Research Part C: Emerging Technologies* 76, 51–70.
- City of Chicago, 2019a. Taxi Trips - 2019. Retrieved July 1, 2022, from <https://data.cityofchicago.org/Transportation/Taxi-Trips-2019/h4cq-z3dy>.
- City of Chicago, 2019b. Transportation Network Providers - Trips - 2019. Retrieved July 1, 2022, from <https://data.cityofchicago.org/Transportation/Transportation-Network-Providers-Trips-2019/iu3g-qa69>.
- Daganzo, C.F., 1994. The cell transmission model: A dynamic representation of highway traffic consistent with the hydrodynamic theory. *Transportation Research Part B: Methodological* 28, 269–287.
- Daganzo, C.F., Geroliminis, N., 2008. An analytical approximation for the macroscopic fundamental diagram of urban traffic. *Transportation Research Part B: Methodological* 42, 771–781.
- Daganzo, C.F., Ouyang, Y., 2019a. A general model of demand-responsive transportation services: From taxi to ridesharing to dial-a-ride. *Transportation Research Part B: Methodological* 126, 213–224. URL: <https://www.sciencedirect.com/science/article/pii/S0191261518307793>, doi:<https://doi.org/10.1016/j.trb.2019.06.001>.
- Daganzo, C.F., Ouyang, Y., 2019b. *Public transportation systems: Principles of system design, operations planning and real-time control*. World Scientific.
- Daganzo, C.F., Ouyang, Y., Yang, H., 2020. Analysis of ride-sharing with service time and detour guarantees. *Transportation Research Part B: Methodological* 140, 130–150. URL: <https://www.sciencedirect.com/science/article/pii/S0191261520303660>, doi:<https://doi.org/10.1016/j.trb.2020.07.005>.
- Di Febraro, A., Gattorna, E., Sacco, N., 2013. Optimization of dynamic ridesharing systems. *Transportation research record* 2359, 44–50.
- Furuhata, M., Dessouky, M., Ordóñez, F., Brunet, M.E., Wang, X., Koenig, S., 2013. Ridesharing: The state-of-the-art and future directions. *Transportation Research Part B: Methodological* 57, 28–46.
- Hart, W.E., Watson, J.P., Woodruff, D.L., 2011. Pyomo: modeling and solving mathematical programs in python. *Mathematical Programming Computation* 3, 219–260.
- Jacob, J., Roet-Green, R., 2021. Ride solo or pool: Designing price-service menus for a ride-sharing platform. *European Journal of Operational Research* 295, 1008–1024.
- Ke, J., Yang, H., Li, X., Wang, H., Ye, J., 2020. Pricing and equilibrium in on-demand ride-pooling markets. *Transportation Research Part B: Methodological* 139, 411–431.
- Kraft, D., 1988. A software package for sequential quadratic programming. *Forschungsbericht- Deutsche Forschungs- und Versuchsanstalt für Luft- und Raumfahrt* .
- Krueger, R., Rashidi, T.H., Rose, J.M., 2016. Preferences for shared autonomous vehicles. *Transportation research part C: emerging technologies* 69, 343–355.
- Lei, C., Jiang, Z., Ouyang, Y., 2020. Path-based dynamic pricing for vehicle allocation in ridesharing systems with fully compliant drivers. *Transportation Research Part B: Methodological* 132, 60–75.

- URL: <https://www.sciencedirect.com/science/article/pii/S019126151831141X>, doi:<https://doi.org/10.1016/j.trb.2019.01.017>. 23rd International Symposium on Transportation and Traffic Theory (ISTTT 23).
- Li, S., Yang, H., Poolla, K., Varaiya, P., 2021. Spatial pricing in ride-sourcing markets under a congestion charge. *Transportation Research Part B: Methodological* 152, 18–45.
- Li, Z., Hong, Y., Zhang, Z., 2016. An empirical analysis of on-demand ride sharing and traffic congestion, in: *Proc. International Conference on Information Systems*.
- Little, J.D., 1961. A proof for the queuing formula: $L = \lambda w$. *Operations research* 9, 383–387.
- Liu, Y., Ouyang, Y., 2021. Mobility service design via joint optimization of transit networks and demand-responsive services. *Transportation Research Part B: Methodological* 151, 22–41. URL: <https://www.sciencedirect.com/science/article/pii/S0191261521001168>, doi:<https://doi.org/10.1016/j.trb.2021.06.005>.
- Makhorin, A., 2008. Glpk (gnu linear programming kit). <http://www.gnu.org/s/glpk/glpk.html>.
- Ouyang, Y., Yang, H., Daganzo, C.F., 2021. Performance of reservation-based carpooling services under detour and waiting time restrictions. *Transportation Research Part B: Methodological* 150, 370–385.
- Özkan, E., Ward, A.R., 2020. Dynamic matching for real-time ride sharing. *Stochastic Systems* 10, 29–70.
- Santi, P., Resta, G., Szell, M., Sobolevsky, S., Strogatz, S.H., Ratti, C., 2014. Quantifying the benefits of vehicle pooling with shareability networks. *Proceedings of the National Academy of Sciences* 111, 13290–13294.
- Shen, S., Ouyang, Y., Ren, S., Zhao, L., 2021. Path-based dynamic vehicle dispatch strategy for demand responsive transit systems. *Transportation Research Record* 2675, 948–959.
- Storch, D.M., Timme, M., Schröder, M., 2021. Incentive-driven transition to high ride-sharing adoption. *Nature communications* 12, 1–10.
- Tafreshian, A., Masoud, N., Yin, Y., 2020. *Frontiers in service science: Ride matching for peer-to-peer ride sharing: A review and future directions*. *Service Science* 12, 44–60.
- Virtanen, P., Gommers, R., Oliphant, T.E., Haberland, M., Reddy, T., Cournapeau, D., Burovski, E., Peterson, P., Weckesser, W., Bright, J., van der Walt, S.J., Brett, M., Wilson, J., Millman, K.J., Mayorov, N., Nelson, A.R.J., Jones, E., Kern, R., Larson, E., Carey, C.J., Polat, İ., Feng, Y., Moore, E.W., VanderPlas, J., Laxalde, D., Perktold, J., Cimrman, R., Henriksen, I., Quintero, E.A., Harris, C.R., Archibald, A.M., Ribeiro, A.H., Pedregosa, F., van Mulbregt, P., SciPy 1.0 Contributors, 2020. *SciPy 1.0: Fundamental Algorithms for Scientific Computing in Python*. *Nature Methods* 17, 261–272. doi:10.1038/s41592-019-0686-2.
- Wang, H., Yang, H., 2019. Ridesourcing systems: A framework and review. *Transportation Research Part B: Methodological* 129, 122–155.
- Wang, X., Agatz, N., Erera, A., 2018. Stable matching for dynamic ride-sharing systems. *Transportation Science* 52, 850–867.
- Xu, Z., Chen, Z., Yin, Y., Ye, J., 2021a. Equilibrium analysis of urban traffic networks with ride-sourcing services. *Transportation science* 55, 1260–1279.
- Xu, Z., Yin, Y., Chao, X., Zhu, H., Ye, J., 2021b. A generalized fluid model of ride-hailing systems. *Transportation Research Part B: Methodological* 150, 587–605.
- Yu, B., Ma, Y., Xue, M., Tang, B., Wang, B., Yan, J., Wei, Y.M., 2017. Environmental benefits from ridesharing: A case of beijing. *Applied energy* 191, 141–152.
- Zeng, W., Han, Y., Sun, W., Xie, S., 2020. Exploring the ridesharing efficiency of taxi services. *IEEE Access* 8, 160396–160406.
- Zhang, K., Nie, Y.M., 2021. To pool or not to pool: Equilibrium, pricing and regulation. *Transportation Research Part B: Methodological* 151, 59–90.
- Zhu, Z., Ke, J., Wang, H., 2021. A mean-field markov decision process model for spatial-temporal subsidies in ride-sourcing markets. *Transportation Research Part B: Methodological* 150, 540–565.
- Zhu, Z., Qin, X., Ke, J., Zheng, Z., Yang, H., 2020. Analysis of multi-modal commute behavior with feeding and competing ridesplitting services. *Transportation Research Part A: Policy and Practice* 132, 713–727.
- Zoepf, S.M., Chen, S., Adu, P., Pozo, G., 2018. The economics of ride-hailing: Driver revenue, expenses and taxes. *CEEPR WP* 5, 1–38.